RPN 101

LABORATORY OF PLASMA STUDIES

CORNELL UNIVERSITY

ITHACA, NEW YORK 14850

PLASMA HEATING BY INTENSE RELATIVISTIC BEAMS DUE TO THE TWO-STREAM INTERACTION

By

L.E. Thode and R.N. Sudan

LPS 96 September 1972

This work is supported by the Office of Naval Research, Contract No. N00014-67-A-0077-0025, and in part by the Atomic Energy Commission, Contract No. AT(11-1)3170-MOD-3.

PLASMA HEATING BY INTENSE RELATIVISTIC BEAMS DUE TO THE TWO-STREAM INTERACTION

by

L. E. Thode and R. N. Sudan
Laboratory of Plasma Studies
Cornell University
Ithaca, New York 14850

Abstract

A theory of the relativistic beam plasma interaction is presented and compared with a one-dimensional computer simulation experiment. We assume the beam interacts with an unstable wave spectrum so narrow that it may be regarded as a single wave. From a qualitative analysis of this model, we obtain the maximum electric field energy to be given by $W \equiv |E_M|^2/16\pi n_b mc^2\gamma_o = \frac{1}{2} S\ (1+S)^{-5/2}$ where $S \equiv \beta_o^2 \gamma_o (n_b/2n_e)^{1/3}$ is a strength parameter, n_b and n_e are beam and plasma electron densities respectively, $\beta_o = v_o/c$, $\gamma_o = (1-\beta_o^2)^{-\frac{1}{2}}$, and v_o is the mean beam velocity. The numerical experiments show that $W = 0.158\ S$ for $S \lesssim 0.6$; reaches a maximum $W \sim 0.1$ at $S \sim 0.6$, and decreases monotonically for $S > 0.6$. The theoretical expression agrees with these results except for $S \ll 1$ where indeed the single wave model may be breaking down because the spectrum is not being totally dominated by one wave. The decrease in energy transfer for $S > 0.6$ is the result of beam electrons being distributed over a large energy range during the trapping process, thus reducing their ability to act coherently. Within a few e-folding times before wave saturation, harmonics are generated due to spatial bunching and their energy spectrum is found to obey a power law dependence. The wave spectrum built up as a result of the two-stream instability decays via the

oscillating two-stream instability. During this process the ions provide an efficient coupling for energy transfer from large amplitude, high phase velocity waves to low phase velocity plasma waves which are Landau damped by the plasma. This anomalous heating results in essentially all the energy lost by the beam going into electron heating.

TABLE OF CONTENTS

I. INTRODUCTION

In recent years high current relativistic electron beams have been developed to the state where they can have important applications in the problem of controlled thermonuclear fusion. One direct application of these beams is in the formation of relativisitic coils so that a minimum $|B|$ configuration with closed lines of force can be achieved without internal conductors[1-5]. Due to the very high power and substantial energy content of these beams, 10^{10}~10^{12} watts and 20~100 kilojoule per pulse, their application to heating a plasma to thermonuclear temperatures becomes very attractive. In order to assess the importance of these high current beams for plasma heating, it becomes necessary to make a quantitative evaluation of the interaction of such beams with a plasma.

It has been shown, both theoretically and experimentally, that beams with $\nu/\gamma>1$ will propagate in the presence of a dense plasma. Here we adopt conventional notation: $\nu = Nr_e$, N is the number of beam electrons per unit length, r_e is the classical electron radius, and γmc^2 is the beam energy. In this connection ν/γ may be interpreted as being equivalent to I/I_A where $I_A \equiv 17{,}000\beta\gamma$ amps is the Alfvén critical current and I is the actual beam current. The plasma serves to neutralize the beam electrostatically; in addition, it allows a return current to flow within the cross-section of the beam which neutralizes the beam's magnetic field. The condition for this current neutralization is[6] $a^2/\lambda_E^2 >> 1$. This condition is true even in a magnetized plasma[7]. Here a is the radius of the beam, $\lambda_E \equiv c/\omega_e$ is the skin depth, ω_e and ω_i are the electron and ion plasma frequencies.

The return current is subject to decay due to turbulent dissipative

processes in the plasma. For instance, the current driven ion sound instability will result in a decrease in the plasma conductivity. However, any reduction in the return current must be accompanied by an increase in the net magnetic field, which in turn gives rise to an inductive axial electric field. The electric field attempts to maintain the return current and thus decelerates the beam. In this manner the beam energy is converted into plasma thermal energy. This heating mechanism was proposed by Lovelace and Sudan[8]. The beam can also transfer its energy to the plasma via the two-stream instability. The present work is devoted to a detailed discussion, supported by computer simulation studies, of this mechanism for a homogeneous beam-plasma system.

For purposes of our present study we assume that the beam propagates in the plasma without any signs of gross magnetohydrodynamic instability. In other words, we assume the growth times of such perturbations to be much longer than those associated with the two-stream instability. This appears to be a reasonable assumption in light of growth times found by Ivanov and Rudakov[9] for the hose and pinch instability.

In Section II we discuss the linear theory of the two-stream instability. We present two cases in which it is possible to represent the unstable wave spectrum by a one-dimensional model. In the first case we consider beam propagation along a strong, magnetic guide field. For beams with $\Delta v_\perp/c \ll 1$ and $\Delta v_{||}/c \ll \gamma_o^{-1}(n_b/2n_e)^{1/3}$, we find the one-dimensional model to be valid provided $\Omega_e^2/\omega_e^2 \geq 10$ and $\Omega_e/\omega_e \geq \gamma_o S$. Here $\Delta v_\perp$ and $\Delta v_{||}$ are the velocity spreads perpendicular and parallel to the direction of beam propogation, $(\gamma_o - 1)mc^2$ is the kinetic energy of the beam, n_e and n_b are the plasma and beam densities,

and $\Omega_e \equiv eB_o/mc$ is the electron cyclotron frequency. In addition, we have defined $S \equiv \beta_o^2 \gamma_o (n_b/2n_e)^{1/3}$ as a strength parameter for the interaction.

The second case is characterized by a spread in perpendicular velocities sufficient to stabilize the faster growing waves which have a finite component of perpendicular wave number $k_\perp$. If initially the spread in perpendicular velocities is not sufficient to stabilize the transverse instabilities, i.e. $\Delta v_\perp/c << (n_b/2\gamma_o n_e)^{1/3}$, then Fainberg, Shapiro, and Shevchenko[10] have shown, through a quasilinear analysis, that there is a rapid increase in perpendicular pressure due to the generation of waves with finite $k_\perp$. During this buildup the beam transfers on the order of $0.25(n_b/2\gamma_o n_e)^{1/3}$ of its initial energy to these plasma modes. However, due to the large longitudinal mass, $m_{||} = \gamma_o^3 m$, no significant velocity spreading takes place in that direction during this time, even though a significant momentum spread, $\Delta p_{||}/p_o \sim 0.59(n_b/2\gamma_o n_e)^{1/3}$ where p_o is the mean beam momentum, is produced. The subsequent beam relaxation then proceeds in the longitudinal direction analogous to a one-dimensional model.

In our treatment we will assume that either a guide field of sufficient strength is present or the beam has a sufficient perpendicular velocity spread to quench the fast transverse instability, initially or as a result of the dynamical action of the transverse wave spectrum. We will thus confine our study to the time evolution of a one-dimensional spectrum.

In Section III the nonlinear theory is discussed. The primary question is what fraction of initial beam energy $W \equiv \sum_k |E_k|^2/8\pi n_b \gamma_o mc^2$ is converted into the electric field energy of the plasma waves during the two-stream instability. For a low energy, high density beam interacting with a warm

plasma a quasilinear analysis of a one-dimensional spectrum by Fainberg et al[10] yields

$$W = 0.158\ S \quad \text{for} \quad S \ll 1 \tag{1}$$

and

$$W \sim 1 \quad \text{for} \quad S \gtrsim 1. \tag{2}$$

Here S has been defined previously as the strength parameter of the interaction. When a high energy, low density beam interacts with a cold plasma the single wave model[11,12] of the interaction is applicable. The single wave model assumes the unstable spectrum is dominated by the wave with the largest linear growth rate. Under these conditions the wave amplitude is limited by particle trapping. Kovtun and Rukhadze[13] treated the single wave model of the interaction and solved Poisson's equation in the frame of the large amplitude wave. The analysis used fluid equations and was restricted to the $S \ll 1$ regime. Their results were[14]

$$W = 0.198\ S \quad \text{for} \quad S \ll 1. \tag{3}$$

However, we point out a possible inconsistency in the method used to obtain the above result.

From a qualitative analysis of the problem we propose the general relationship

$$W = 0.5\ S(1+S)^{-5/2} \quad \text{for all } S. \tag{4}$$

This result is surprising in the sense that a maximum is predicted when $S \approx 0.66$. (For example, a 1.5 Mev beam with a beam to plasma density ratio of 10^{-2} has a strength parameter of $S = 0.62$.) The decrease in energy transfer for $S > 0.66$ is due to an increase in the spread of frequencies with which trapped beam electrons oscillate in the potential well of the

wave and, consequently, a decrease in coherent energy transfer to the wave. Note that the result is in marked contrast to the Fainberg et al[10] results for $S \gtrsim 1$.

In Section IV the results of a one-dimensional, electrostatic numerical experiment are presented. A summary of the eleven cases performed is given in Table 1. The typical evolution of the interaction is found to occur in basically three stages. In the first stage there is exponential growth of waves in agreement with the linear theory of the two-stream instability. This exponential growth ceases abruptly when the beam electrons trapped near the bottom of the potential well of the large amplitude wave complete one-half revolution in phase space. The maximum of W occurs at $S \approx 0.6$. For $S \lesssim 0.6$ the dependence is linear, $W = 0.158\ S$ in agreement with the quasilinear results of Fainberg et al[10]. For $S \gtrsim 0.6$, W decreases in good agreement with (4).

There are situations in which the large amplitude wave can significantly accelerate some fraction of the background electrons. The additional damping introduced by the acceleration of the plasma electrons causes a reduction in the limiting amplitude of the wave when $\omega_E^2/\omega_e^2 \gtrsim 0.038$ where $\omega_E^2 \equiv 4\pi e^2 n_e/\gamma_W^3 m$ is the effective beam plasma frequency, $\gamma_W = (1 - (\omega/k_o c)^2)^{-\frac{1}{2}}$, and ω/k_o is the phase velocity of the large amplitude wave. Also, within a few e-folding times of wave saturation, harmonic generation is present due to spatial bunching. The power law dependence for the energy spectrum of the harmonics is found to be $|E_{k=nk_o}|^2 = |E_{k_o}|^2\ n^{-\alpha}$ where k_o is the wave number of the fundamental and n is the harmonic number. The exponent α is typically 4.75 ± 0.50 indicating a much faster decay than in the nonrelativistic case. During this stage adiabatic heating of the electron and ions takes place.

The second stage begins shortly after saturation with the wave energy oscillating about a mean value with frequency $\omega_T = (ek_o E_{k_o}/\gamma_W^3 m)^{\frac{1}{2}}$. At this point the large amplitude wave can be regarded as being equivalent to an external driver wave capable of exciting parametric instabilities in the plasma. Indeed, after a few amplitude oscillations the wave decays via the oscillating two-stream instability to a much lower level. This instability produces low phase velocity waves traveling parallel and antiparallel to the direction of beam propagation. The electron waves are then Landau damped by plasma producing heavily populated, energetic tails on the electron distribution and to a much lesser extent on the ion distribution. During this process essentially all the energy lost by the beam goes into electron heating. The final stage corresponds to resonant heating.

II. LINEAR THEORY

In order to claim some degree of validity for a one-dimensional model of the two-stream instability spectrum, we consider regimes in which the maximum growth rate of the two-stream instability $0.866\gamma_o^{-1}(n_b/2n_e)^{1/3}\omega_e$ is at least twice as large as the growth rate of any mode involving a finite $k_\perp$.

A) Beam Propagation Along a Strong Magnetic Guide Field.

We restrict the analysis to regions sufficiently far behind the beam front to insure both electrostatic and magnetic neutralization. Therefore, we can neglect the self magnetic field in comparison with the guide field. Since at this point we are only interested in offering an argument for making the one-dimensional model plausible, we assume that the waves are predominantly electrostatic. The linear dispersion relationship for these waves can be expressed as

$$\varepsilon(\underline{k},\omega) = 1 + \sum_j \mu_j(\underline{k},\omega) = 0$$

where $\mu_j(\underline{k},\omega)$ is the susceptibility of species j, j = i, e, and b for ions, electrons and beam electrons.

Restricting the analysis to the high frequency regime, $\omega > (\omega_e\Omega_e)^{1/2}$, the ion contribution can be neglected. Choosing a maxwellian distribution for the electrons, with a characteristic thermal velocity $v_e = (T_e/m)^{1/2}$, the electron susceptibility can be written in the form

$$\mu_e = -\frac{\omega_e^2}{\omega^2}\cos^2\theta - \frac{\omega_e^2}{\omega^2-\Omega_e^2}\sin^2\theta \qquad (5)$$

for $k_\perp v_e/\Omega_e \lesssim 0.20$. Here $\cos\theta = k_{||}/k$ and $k^2 = k_\perp^2 + k_{||}^2$. The relativistic nature of the beam electrons can be accounted for by the two mass approximation, $m_{||} = \gamma^3 m$ and $m_\perp = \gamma m$. The beam distribution function can then be approximated by $f_b = (2\pi\theta_\perp)^{-1}\,\delta(u_o - u_{||})\exp(-u_\perp^2/2\theta_\perp^2)$ where $\underline{u} = \gamma\underline{v}$, $\theta_\perp = \gamma^2(\Delta v_\perp)^2$, $\gamma =$

$(1 + u_o^2/c^2)^{1/2}$, and $\Delta v_\perp$ is the spread in perpendicular velocities. Under these assumptions, the beam susceptibility becomes

$$\mu_b = -\frac{\omega_{b\perp}^2 \sin^2\theta}{(\omega - k_\parallel v_o)^2 - \Omega_R^2} - \frac{\omega_{b\parallel}^2 \cos^2\theta}{(\omega - k_\parallel v_o)^2} \qquad (6)$$

where $\omega_{b\perp}^2 = \omega_b^2/\gamma_o$, $\omega_{b\parallel}^2 = \omega_b^2/\gamma_o^3$, $\Omega_R = \Omega_e/\gamma_o$ is the relativistic cyclotron frequency, and $k_\perp \Delta v_\perp/\Omega_R \lesssim 0.20$.

If we take $n_b/\gamma_o n_e \ll 1$, which is the typical situation, then the normal modes of the system are mainly determined by

$$1 + \mu_e = 0. \qquad (7)$$

For $\omega_e^2/\Omega_e^2 \ll 1$ there are two natural frequencies corresponding to (7):

$$\omega^- = \omega_e \cos\theta$$

and

$$\omega^+ = \Omega_e(1 + \omega_e^2 \sin^2\theta/2\Omega_e^2).$$

We expect instability to occur whenever

$$\omega^\pm \approx k v_o \cos\theta - n\Omega_R \quad \text{with} \quad n = 0, \pm 1 .$$

The maximum growth rates δ_n^α ($\alpha = \pm$ for $\omega \approx \omega^\pm$) corresponding to the above resonances are (see Appendix A for details):

$$\delta_o^+/\omega_e = \frac{\sqrt{3}}{2\gamma_o} (n_b/2n_e)^{1/3} (\omega_e/\Omega_e)^{1/3} \sin^{2/3}\theta \cos^{2/3}\theta$$

$$\delta_o^-/\omega_e = \frac{\sqrt{3}}{2\gamma_o} (n_b/2n_e)^{1/3} \cos\theta$$

$$\delta^{+}_{-1}/\omega_e = \frac{1}{2}\,(n_b/n_e)^{1/2}\ \ (\omega_e/\Omega_e)\,\sin^2\theta$$

$$\delta^{-}_{-1}/\omega_e = \frac{1}{2}\,(n_b/n_e)^{1/2}\ (\omega_e/\Omega_e)^{1/2}\,\sin\theta\cos^{1/2}\theta$$

The resonance $\omega^{\pm} \approx kv_o \cos\theta + \Omega_R$ is found to be stable. Thus, the spectrum will be approximately one dimensional if $\Omega_e^2/\omega_e^2 \gtrsim 10$ and $\Omega_e/\omega_e \gtrsim \gamma_o S$. Under these restrictions the dispersion relationship reduces to

$$1 - \frac{\omega_e^2}{\omega^2}\cos^2\theta \;-\; \frac{\omega_{b||}^2\cos^2\theta}{(\omega - k_{||}v_o)^2} = 0$$

with the maximum growth rate occurring for waves with $k_\perp = 0$.

B) A Beam in Which the Transverse Instabilities Have Been Stabilized by a Spread in Perpendicular Velocities.

It is possible to stabilize modes with finite $k_\perp$ provided the beam has a sufficiently large spread in its transverse velocities $\Delta v_\perp$. However, if initially $\Delta v_\perp$ is small, i.e. $\Delta v_\perp/c \ll (n_b/\gamma_o n_e)^{1/3}$, then the maximum growth rate is[10] $\delta = 0.866\,(n_b/2\gamma_o n_e)^{1/3}\omega_e$ which occurs for waves with $k_{||}^2/k_\perp^2 = 1.06\,(2\gamma_o n_e/n_b)^{1/3}\ \Delta v_\perp/c \ll 1$. As the instability progresses, $\Delta v_\perp$ increases until $\Delta v_\perp/c \sim (n_b/\gamma_o n_e)^{1/3}$. During this time the fraction of beam energy converted into electric field energy associated with the transverse waves is approximately $0.25\,(n_b/2\gamma_o n_e)^{1/3}$. The important point, however, is that the velocity spread in the parallel direction $\Delta v_{||}$ is not significantly increased during this process due to the large effective mass in that direction. Thus after the saturation of the transverse modes, the remaining beam

instability follows the simple one-dimensional dispersion relation

$$1 - \frac{\omega_e^2}{\omega^2} - \frac{\omega_{b||}^2}{(\omega - kv_o)^2} = 0 \ . \qquad (8)$$

This, of course, assumes that the growth rate in the longitudinal direction exceeds any growth rates associated with perpendicular modes of a warm beam.

At this point, we will assume expression (8) adequately describes the linear evolution of the interaction and recall that the growth rate and frequency of the most unstable wave is given by

$$\omega_{k_o} = 0.866\gamma_o^{-1}(n_b/2n_e)^{1/3}\omega_e$$

$$\delta_{k_o} = \omega_e(1 - 0.5\gamma_o^{-1}(n_b/2n_e)^{1/3})$$

for $n_b/\gamma_o^3 n_e << 1$. To facilitate comparison between theory and computer experiments equation (8) was solved numerically for a wide range of parameters[15]. Typical plots of ω_k and δ_k as a function of wave number are given in Fig. 1.

III. NONLINEAR THEORY

A) Energy Transfer During Two-Stream Instability Phase.

We consider an infinitely long one-dimensional beam-plasma system. In practice, this requires the interaction distance L to be much greater than the wavelength of the fastest growing wave. In addition, we require $L >> L_n$ where L_n is the distance over which the two-stream instability can develop to its nonlinear limit. We can estimate L_n by noting that a strong hydrodynamic instability, such as the two-stream instability, may e-fold up to ten times. Here the number of e-folding times is defined as $N \equiv 0.866\ \gamma_o^{-1}(n_b/2n_e)^{1/3}\ \omega_e t_s = \ell n\ (\phi_M/\phi_T)$ where ϕ_M is the amplitude of the potential at the time of saturation, ϕ_T is the amplitude of the thermal noise, and t_s is the total time the instability grows at an exponential rate. Therefore, chosing N = 10 we estimate $L_n \approx 11.55\lambda_E\ \gamma_o\ (2n_e/n_b)^{1/3}$. For example, if a 0.5 Mev beam with a density of $10^{11}/cm^3$ interacts with a plasma of density $10^{13}/cm^3$ then $L_n \approx 23cm$.

Initially we assume the beam thermal velocity $\Delta v_{||}$ to be small[16] such that $\Delta v_{||}/c << \gamma_o^{-1}(n_b/2n_e)^{1/3}$. Extending an argument given by O'Neil et al[12] to the relativistic regime, the half width of the wave spectrum after N e-folding times is approximately $\delta k/k_o \approx 1.76\ \gamma_o^{-1}\ (n_b/2n_e)^{1/2}\ N^{-1/2}$ where k_o is the wave number corresponding to the most unstable wave. Thus for a low energy, high density beam interacting with a warm plasma, the spectrum may be composed of enough waves of varying phases so that a quasilinear analysis to determine the saturation level of the waves is possible. On the other hand, for a high energy, low density beam interacting with a cold plasma, the wave spectrum can be very narrow. In this limit, the spectrum may be approximated by a single wave with wave number k_o.[11,12,17,18] In this report we are pre-

dominantly concerned with the single wave model of the interaction.

In the analysis of Kovtun and Rukhadze[13], the background plasma is treated in the linear approximation, and the determination of the limiting amplitude of wave reduces to the solution of a harmonic oscillator being driven by a small nonlinear term associated with the beam. Using the asymptotic methods of Krylov-Bogolyubov and limiting their analysis to the $S \ll 1$ regime, they obtained the relationships

$$1 - \frac{\omega_e^2}{\omega^2} - \frac{\omega_b^2}{\gamma_o^3(\omega-kv)^2 + 2e\phi\, k^2/m} N(\xi) = 0 \quad \text{for } \xi < 1 \qquad (9)$$

and

$$1 - \frac{\omega_e^2}{\omega^2} + \frac{2\omega_b^2 m}{e\phi\, k^2}\left[1 - 2\frac{E(1/\xi)}{K(1/\xi)}\right] = 0 \qquad \text{for } \frac{1}{\xi} < 1. \qquad (10)$$

In the above expressions, ϕ is the amplitude of the potential in the laboratory frame, $N(\xi) = 8\xi^{-4}(2-\xi^2 - 2E(\xi)/K(\xi))$, K and E are the complete elliptic integrals of the first and second kind, and $\xi = 2e\phi\,(\frac{1}{2}m\gamma_o^3(\omega/k - v)^2 + e\phi)^{-1}$ is a trapping parameter. Expressions (9) and (10) are nonlinear dispersion relationships which take into account the finite amplitude of the wave. The maximum amplitude of the potential is taken to occur at $\xi = 1$: when particle trapping is complete. At this point, there are three relationships between ϕ, ω, and v; namely,

$$1 - \frac{\omega_e^2}{\omega^2} - \frac{\omega_b^2}{\gamma_o^3(\omega-k_o v)^2 + 2e\phi_M k_o^2/m} = 0, \qquad (9')$$

$$e\phi_M = \frac{2m\omega_b^2}{\omega_e^2-\omega^2} \quad \frac{\omega^2}{k_o^2} \quad , \tag{10'}$$

and

$$\tfrac{1}{2}m\gamma_o^3 \, (\omega/k_o - v)^2 = e\phi_M \tag{11}$$

where ϕ_M is now the maximum amplitude of the potential. Using condition (11), one can find three roots corresponding to the frequency from Equation (9'). However, at the time of saturation none of the roots make any physical sense. Thus (9') was ignored completely, and (10') and (11) were combined to obtain

$$1 - \frac{\omega_e^2}{\omega^2} + \frac{4\omega_b^2}{\gamma_o^3(\omega - k_o v)^2} = 0 \tag{12}$$

from which

$$\omega = \omega_e(1 - 2^{2/3}\gamma_o^{-1}(n_b/2n_e)^{1/3}) \tag{13}$$

and $\delta = 0$. Here it was assumed that the condition $k_o v \approx \omega_e$ remains valid throughout the interaction. Substituting the frequency (13) into the expression for the potential (10') and noting that $\sum_k |E_K|^2/8\pi \approx k_o^2\phi_M^2/16\pi$ one finally obtains[14]

$$W \equiv |E_M|^2/16\pi n_b \gamma_o mc^2 = 0.198\ S \qquad \text{for } S \ll 1. \tag{14}$$

We have used the method outlined above to calculate the fraction of energy lost by a nonrelativistic beam during the two-stream instability. We must assume that the beam velocity spread as a result of the instability remains small compared to the initial beam velocity since we need the condition

$k_o v \approx k_o v_o \approx \omega_e$ to remain valid. We find that $|E_M|^2/8\pi n_b m v_o^2 = 0.316\ (n_b/n_e)^{1/3}$; however, the nonrelativistic results of references (11), (12), (17), and (18) indicate that the constant of proportionality is 0.96 to 1.125. Also, we note that at the time of saturation, the frequency shift $\omega - \omega_e \equiv \Delta\omega$ of the large amplitude wave predicted by the above method, $\Delta\omega = -3.16\Delta\omega_L$, is much larger than that found by O'Neil et al[12], $\Delta\omega = -1.2\Delta\omega_L$. Here $\Delta\omega_L = 0.5\ (n_b/2n_e)^{1/3}\omega_e$ is the magnitude of the frequency shift predicted by linear theory. Consequently, we are skeptical of expression (14) since it does not agree in the nonrelativistic limit with other calculations.

We now present a qualitative analysis which embraces the entire range of the parameter S. To start we note that

$$\gamma_W = (1-\beta_W^2)^{-\frac{1}{2}} \approx \gamma_o(1+S)^{-\frac{1}{2}} \qquad (15)$$

where we have used the linear result for the frequency, $\omega=\omega_e(1-0.5\gamma_o^{-1}(n_b/2n_e)^{1/3})$, and $\beta_W = \omega\beta_o/k_o v_o$. Also a term of order $(n_b/2n_e)^{2/3}$ has been neglected compared to unity. Therefore, the energy difference between a particle moving with velcotiy v_o and one that moves with the wave phase velocity increases as S increases. Our analysis, in some respects, is similar to that presented by Drummond et al[11] for the nonrelativistic case.

The evolution of the wave growth and saturation is depicted in the laboratory frame phase space plots of Figs. 2a, 2b, and 2c. At $t = t_o$ (see Fig. 2a) the beam electrons move over a single wave with relative velocity

$$\Delta v_W/c = 0.5\gamma_o^{-1}\beta_o(n_b/2n_e)^{1/3} \quad (1 - \omega v_o/kc^2)^{-1}. \qquad (16)$$

At $t = t_1$ (see Fig. 2b) trapping of the beam electrons begins when the separatrix associated with the potential $\phi(t_1)$ passes through the actual beam trajectory. At this time, the beam trajectory is still essentially a straight line ($\Delta p/p_o \approx 0.1$) since the field has not had sufficient time to modify the beam electron momentum. In Fig. 3 the separatrix is plotted in the wave frame for various values of $\Delta v_W/c$. Note that as $\Delta v_W/c$ increases, or equivalently S, the separatrix tends to become sharper. Due to the increasing sharpness of the separatrix, the initial number of beam electrons trapped at $t = t_1$ decreases as S increases. After being trapped, the electrons begin to rotate in phase space giving up their laboratory frame kinetic energy to the wave. In the meantime, the wave is continually trapping more electrons as its amplitude increases. At $t = t_2$ (see Fig. 2c) the electrons trapped at $t = t_1$ have completed one-half revolution in phase space. At this time the wave has grown to such a large amplitude that it has trapped most of the remaining electrons. As in the nonrelativistic case, the wave growth ceases at this point. Due to relativisitc effects, however, electrons trapped after $t = t_1$ will be rotating in phase space more slowly than in the nonrelativistic case. For example, a nonrelativistic particle trapped half way up the potential well has a trapping frequency in the laboratory frame of $\omega_T = 0.85\ (ek_o^2\phi_M/m)$ while a relativistic particle similarly trapped, with $\gamma_M = 2$ say, has a trapping frequency of $\omega_T = 0.68\ (ek_o^2\phi_M/\gamma_W^3 m)$. The trapping frequencies are discussed in Appendix B. Here $(\gamma_M - 1)mc^2$ is the maximum particle kinetic energy in the wave frame. As a

result of a greater spread in trapping frequencies, fewer electrons lose their energy coherently to the wave[19]. Thus, in the relativistic case, the number density δn_b of electrons losing their energy coherently to the wave is approximately the number density of electrons trapped near the bottom of the well.

In order to estimate δn_b we assume the momentum distribution in the laboratory frame is smeared symmetrically about $\bar{u}$ over a range of $2\Delta u$ (see Fig. 5a) where $\bar{u}$ is below u_o by the amount of momentum imparted to the waves. Given the momentum distribution $f(u)$, the velocity distribution can be found from the relationship $dn = f(u)du = f(v)dv$ where dn is the electron density between $v - dv/2$ and $v + dv/2$. In this manner we find $f(v) = \gamma^3(v)$ and thus

$$dn = \frac{n_b}{2\Delta u} \cdot \gamma^3(v)dv \tag{17}$$

where we have used $f(u) = n_b/2\Delta u$ (Recall that $u=p/m=\gamma v$). We assume that the density of electrons losing a good fraction of their laboratory frame energy to the wave is given by

$$\delta n_b \approx \frac{n_b}{2\Delta u} \gamma_W^3 \Delta v. \tag{18}$$

This is a reasonable assumption since most of the energy lost by an electron occurs before its velocity drops below the phase velocity of the wave (see Fig. 6). Initially, $u_o >> 1$ and the momentum spread can be approximated by $\Delta u \approx \gamma_o^3 \Delta v_o$. Expression (18) can then be rewritten in the form $\delta n_b/n_b \approx (\gamma_W/\gamma_o)^3 \Delta v/2\Delta v_o$. In the nonrelativistic limit $\delta n_b/n_b \to 1$ and $\gamma_W \to \gamma_o$ requiring $\Delta v/2\Delta v_o = 1$ (see Fig. 5b). We expect $\Delta v/2\Delta v_o$ to be only weakly dependent on S so that we may approximate it by unity in what follows[20]. Thus, we finally obtain

$$\delta n_b = \frac{\gamma_W^3}{\gamma_o^3} \cdot n_b \quad . \tag{19}$$

It now remains to determine the laboratory frame kinetic energy lost by one electron after one half revolution in phase space. Referring to Fig. 2c, the laboratory frame energy in rest mass units of an electron at point Q_1 is $\gamma_1 = \gamma\gamma_W(1+\Delta\beta_W\beta_W)$ and at point Q_2 is $\gamma_2 = \gamma\gamma_W(1-\Delta\beta_W\beta_W)$ where $\Delta\beta_W = \Delta v_W/c$ is given by (16), $\gamma = (1-(\Delta\beta_W)^2)^{-\frac{1}{2}}$, and $\beta_W = \omega/k_o c$. Therefore, the kinetic energy lost is $\Delta K.E. = (\gamma_1-\gamma_2)mc^2 = 2\gamma\gamma_W\Delta\beta_W\beta_W mc^2$. At this point we want to obtain $\Delta K.E.$ only in terms of S and thus use the relationship $2\gamma\Delta\beta_W\beta_W \leq S(1+S)^{-\frac{1}{2}}$ (see Appendix C) to obtain

$$\Delta K.E. = \gamma_o mc^2 \cdot S(1+S)^{-1} \tag{20}$$

Combining (15), (19), and (20), and recalling that roughly one half of the energy lost by the beam electrons goes into the electric field energy of the wave (the other half goes into the organized motion of the plasma) we obtain the final result

$$W = 0.5S(1+S)^{-5/2} \quad \text{for all S.} \tag{21}$$

As the electrons continue to rotate in phase space they start to regain their laboratory frame energy and the wave amplitude decreases. Thus as the electrons rotate, alternately losing and gaining their energy, the field amplitude will oscillate about some mean value. Since the oscillation in wave amplitude is being controlled by the electrons near the bottom of the potential well, we expect the period of oscillation to be $\tau_{osc} = 2\pi/(ek_o^2\phi_M/\gamma_W^3 m)^{\frac{1}{2}}$. The time evolution of the electric field energy is sketched in Fig. 3.

During the trapping process the beam electrons are rotated from a state of constant velocity to a state of essentially constant position, and the beam charge density becomes rich in spatial harmonic content. It was shown in the work of O'Neil et al[12] that this spatial bunching leads to a power law dependence for the energy spectrum of the spatial harmonics of the form $|E_{k=nk_o}|^2 = |E_{k_o}|^2 n^{-2.5}$. In the relativistic regime we expect the degree of spatial bunching to be reduced as a result of the increased spread in rotational frequencies, and a correspondingly faster decay in the harmonic spectrum.

B) Oscillating Two-Stream Instability and Anomalous Heating Following Wave Saturation.

After saturation the large amplitude waves produced during the two-stream instability can be considered as equivalent to external driver waves which are capable of producing parametric instabilities in the plasma. Since the large amplitude wave frequency is just below the plasma frequency we expect the oscillating two-stream instability to be excited[21,22]. Also the large amplitude wave is subject to the trapped particle instability[23,24]. However, the magnitude of the growth rate for the trapped particle instability is typically less than the trapping frequency. In our case, the trapping frequency is approximately $(ek_o^2\phi_M/\gamma_W^3 m)^{\frac{1}{2}}$ and is small due to relativistic effects. Thus the oscillating two-stream instability is expected to be the dominant instability.

The oscillating two-stream instability produces purely growing ion fluctuations and electron waves traveling parallel and antiparallel to the direction of propagation of the driver wave. The instability is the result of the electrons being driven to and fro across the ions. For a large amplitude wave of the form $E_o \sin \omega_o t$, Sanmartin[22] finds the growth rate to be

$$\delta/\omega_e = ((A^2 + B^2)^{\frac{1}{2}} - A)^{\frac{1}{2}} \qquad (22)$$

when the growth rate is much larger than the ion-electron collision time. In the above expression $A=0.125(\omega_p^2-\omega_o^2)^2 +\mu(1 - 2x^{-1}J_o(x)J_1(x))> 0$ and $B = \mu J_1^2(x)\ (\omega_p^2 - \omega_o^2 + 4\mu x^{-2}\cdot(1 - J_o^2(x)) > 0$ where $\mu = m/2M_i$, $\omega_p^2 = \omega_e^2 + 3k^2v_e^2$, $x = eE_o/m\omega_o v_e$, and J_n is the Bessel function of the first kind.

The electron waves produced as a result of oscillating two-stream instability have much lower phase velocities than the driver wave. This can be seen from the energy and momentum conservation conditions for the waves. Denoting the driver, electron, and ion waves by (ω_o, k_o), (ω_e, k_e), and (ω_i, k_i) the above conditions are $\omega_o = \omega_i + \omega_e$ and $k_o = k_i + k_e$. In the above analysis $k_o \simeq 0$ and $\omega_i \simeq 0$, thus $\omega_e \simeq \omega_o$ and $k_e + k_i \simeq 0$ from which the phase velocity of the electron waves satisfy $v_p = \pm\ \omega_o/|k_e|$ and $|v_p| << \omega_o/k_o$. Therefore, the driver wave can transfer its energy to lower phase velocity waves which are then, in turn, Landau damped by the plasma. This anomalous heating produces heavily populated, energetic tails on the electron distribution and to a lesser extent on the ion distribution, while the driver wave decays to a much lower level[25,26].

IV. NUMERICAL RESULTS

In this section we summarize the results of a series of one-dimensional computer simulations of the collisionless, relativistic beam-plasma interaction[27]. The simulations were performed using an electrostatic particle code[28]: this essentially amounts to following the motion of a large number of electrons and ions in their self-consistent electric field. In this case, the electric field is calculated from the monopole and dipole contributions of the charge density using periodic boundary conditions[29]. The electrons were treated relativistically, but the ions were treated nonrelativistically since the minimum ion to electron mass ratio was five hundred. Initial electron and ion velocity distributions were maxwellians with zero drift velocities, whereas the beam was chosen to be monoenergetic. The system lengths were $512\lambda_D$ and $1024\lambda_D$ where λ_D is the Debye length corresponding to the initial electron temperature. The electron to ion temperature ratio was taken to be 25 in all the runs, and the time step was $0.20\omega_e^{-1}$. In Table 1 the eleven numerical experiments are summarized.

We are interested in determining the amount of heating which can be expected from the direct two-stream interaction. In this study, the average kinetic energy of the electron and ion distributions is adopted as a measure of the heating. It is found that the energy transfer to the plasma occurs in basically three stages with the heating rate decreasing from stage to stage. In the first stage, which occurs during the two-stream instability, adiabatic heating of the plasma takes place. During the second stage, the electric field energy of the large amplitude waves is converted into plasma kinetic energy as a result of parametric instability. By this time, the beam distribution has evolved into a gentle bump, and resonant heating takes

place during the third stage.

In Fig. 7 the growth rate as a function of wave number is plotted for run number four, (R4). (The notation to be used is as follows: (Rn) where n refers to the run number given in Table 1.) In Fig. 7, the dashed line is the numerical solution of Eq. (8), and the solid line is the numerical solution of Eq. (8) with the finite-size of the simulation particles taken into account[30,31]. Note the decrease in growth rate at higher wave numbers due to finite-sized particles. In Table 1, columns 9 and 10 give the maximum growth rates obtained from the dispersion relation and from the simulation experiments. The agreement with linear theory is generally good. The consistently lower growth rates obtained from the simulation experiments are the result of finite-sized particles and the discrete wave number spectrum used in the simulation (the growth rates in parenthesis have taken these factors into account). In Fig. 8, $|E_{k_o}|^2/16\pi n_b \gamma_o mc^2$, $T_e = 0.5 m v^2_{e,r.m.s.}$, $T_i = 0.5 M_i v^2_{i,r.m.s.}$, and $\langle v \rangle_e^2$ are given as a function of time for (R4). Here $\langle v \rangle_e$ and $v_{r.m.s.}$ are the average and root mean square velocity. After $\omega_e t \simeq 50$, the amplitude of the wave with the fastest growth rate is such that it is dominating the plasma electron and ion dynamics, and thus T_e, T_i, and $\langle v \rangle_e^2$ grow at the same rate as the wave. The increase in T_e and T_i is, of course, adiabatic at this stage. The increase in $\langle v \rangle_e$ is due to an average electric field resulting from a growing wave.

In Fig. 9, the mode energy ($|E_m|^2/16\pi n_b \gamma_o mc^2$) shortly before wave saturation is plotted as a function of mode number ($m = L/\lambda_m$) for (R7). Here λ_m is the wavelength corresponding to mode (m) and L is the system length. The spatial harmonic structure is clearly present with the field energy in a

given harmonic decreasing as the harmonic number increases, indicating a possible power law dependence. In Fig. 10, the harmonic field energy ($|E_n|^2/16\pi n_b \gamma_o mc^2$) is plotted as a function of the harmonic number (n) for (R4), (R7), and (R11). A power law dependence exists and the exponent ranges from 4.5 to 5.25 compared to 2.5 for the nonrelativistic case[32].

The maximum electric field energy at the time of saturation of the hydrodynamic two-stream instability is plotted as a function of S in Fig. 11. For $S < 0.6$, $W = 0.158\ S$ which is the dashed line in Fig. 11 and is in agreement with the quasilinear result of Fainberg et al[10]. Note that the result of Kovtun et al[13] is also in fair agreement with the data; however, in view of the discussion in Sec. III, we remain skeptical of that analysis. The qualitative result proposed in this paper, Eq. (4), which is the dark line in Fig. 11, is slightly high for all S; but, it describes the observed data, including the maximum at $S \sim 0.6$ quite well. We also note that for $S < 0.6$, less than 75% of the electric field energy is in the wave with maximum linear growth rate, whereas for $S > 0.6$ over 90% of the electric field energy is in the dominant wave (see column 12 in Table 1). Thus, for $S < 0.6$, the single wave model is breaking down since one wave is not totally dominant. In Fig. 12, the momentum distribution shortly after the time of wave saturation is plotted for (R11), where p_o is the initial momentum. This is to be compared with the momentum distribution sketched in Fig. 5a.

To this point we have tacitly assumed the electron trapping was the sole mechanism in the single wave model of the interaction responsible for limiting the wave amplitude. However, in some parameter regimes, the wave

amplitude has become so large that it can effectively accelerate an appreciable number of plasma electrons. When the net energy loss to the wave as a result of this acceleration exceeds the energy gain, the wave will saturate. In the nonrelativistic regime[17,33], it was found that the electron velocity distribution would merge with the plasma electron distribution during the two-stream instability if $\omega_b^2/\omega_e^2 \gtrsim 0.038$. In Fig. 11, the observed energy transfer for (R4) lies well below the expected value when compared with the rest of the data. In this case, the additional damping produced by the wave accelerating plasma electrons has lowered the saturation level of the wave. In Figs. 13a,13b,14a, and 14b, segments of phase space near the time of wave saturation are shown for (R2), (R4), (R7), and (R11). In cases (R2) and (R4) significant electron acceleration is clearly present. For these two cases, ω_E^2/ω_e^2 is 0.05 and 0.0315 respectively where $\omega_E^2 \equiv 4\pi e^2 n_b/\gamma_W^3 m$ is an effective beam frequency. Note that (R2) is one of the nonrelativistic check runs in which the maximum electric field energy is significantly less than predicted, 0.223 compared to .405. In contrast, for cases (R7) and (R11), Figs. 14a and 14b, ω_E^2/ω_e^2 is 0.0322×10^{-2} and 0.049×10^{-2}. In view of the above data, $\omega_E^2/\omega_e^2 \gtrsim 0.038$ appears to give a rough rule of thumb for predicting when background electron acceleration can significantly effect the saturation level of the wave spectrum.

After saturation the amplitude of the wave spectrum oscillates about a mean value. In Fig. 15, the observed oscillation frequencies are compared to the oscillation frequency associated with the bottom of the potential well of the dominant wave, $\omega_T = (ek_o^2\phi_M/\gamma_W^3 m)^{\frac{1}{2}}$. The curve in Fig. 15 represents a plot of $\omega_T\gamma_W^2/\omega_e$ against $\eta \equiv e\phi k_o/\gamma_W mc^2$. Except for case (R4), the agreement

is within 15% indicating that the electrons near the bottom of the potential well are responsible for the oscillations in the wave amplitude.

During this time we observe an increase in the ion density fluctuations (see Fig. 16), and after, at most, two wave energy oscillation periods, the wave spectrum begins to decay. In Fig. 17, electron and ion phase space are shown at the beginning of the wave spectrum decay for (R7). The electrons are being accelerated out of both sides of the distribution and large ion fluctuations are present. In Fig. 18, the observed growth rates of ion fluctuations are compared with the theoretical growth rates for the oscillating two-stream instability obtained from Eq. (22). The magnitude of the growth rates are in fair agreement except at higher wave numbers. However, since all the waves have basically the same frequency, the Landau damping of a particular wave will increase with larger wave numbers. Thus, we feel the sharp decrease in growth rate for higher wave numbers is due to Landau damping[34]. Indeed, we find the lower phase velocity waves lie in the tail of the electron distribution. In light of the above evidence, the oscillating two-stream instability appears to be the dominant decay mechanism for the high phase velocity waves produced during the two-stream instability.

In Fig. 19, the electron distribution function for (R8) is shown at various times. Time $\omega_e t \simeq 180$ corresponds to the end of the first stage of the interaction. The number of electrons in the tail of the distribution has been increased because of a net acceleration due to the growing wave. This velocity spread occurs only in the direction of beam propagation. Time $\omega_e t = 600$ marks the end of the second stage with the tail of the distribution

having been heavily populated due to anomalous heating. In contrast to the earlier phase $\omega_e t<180$, this increase in velocity occurs in both directions. In Fig. 20, the total electric field energy corresponding to the above case is plotted as a function of $\omega_e t$. The first and second stages are indicated along with the oscillation period of the amplitude oscillations. At the beginning of the third stage the plasma and beam electron distribution corresponds to a bump on the tail situation as shown in Fig. 21 and resonant heating begins.

In Fig. 22 the average electron kinetic energy in units of kev is given as a function of $\omega_e t$ for (R9) and (R11). The average ion kinetic energy increase for (R9) and (R11) over the same period of time as in Fig. 22 was only in the order of a few electron volts. Thus, essentially all the energy lost by the beam has gone into the electrons and the ions merely provide an efficient coupling for energy transfer from high phase velocity waves to lower phase velocity waves via the oscillating two-stream instability. In order to estimate the partitioning of the energy between the bulk of the electrons, which remain nonrelativistic, and the relativistic tails, we plot $0.5mv^2_{r.m.s.}$ in units of kev for (R8), (R9), (R10), and (R11) in Fig. 23. On comparing Fig. 22 and Fig. 23, we observe that although the number of electrons in the relativistic tails of the distribution is substantially smaller than the nonrelativistic portion of the distribution, their energy content represents a large fraction of the total energy.

ACKNOWLEDGMENTS

One of us (L.E.T.) wishes to thank Dr. R. Shanny and Dr. T. Coffey of the Plasma Physics Division at the Naval Research Laboratory, Washington, D. C., for a summer position and the use of the computer facilities to perform the numerical experiment. We acknowledge helpful discussions with Dr. R. Lovelace and Dr. S. Kainer.

This work is supported by the Office of Naval Research, Contract No. N00014-67-A-0077-0025, and in part by the Atomic Energy Commission, Contract No. AT(11-1)3170-MOD-3.

References

1) N. C. Christofilos, Proc. of the 2nd U. N. Int. Conf. on Peaceful Uses of Atomic Energy, 32, 279 (1958).

2) M. Friedman and A. F. Kuckes, Bull. Am. Phys. Soc. 14, 1253 (1969).

3) E. Ott and R. N. Sudan, Phys. Fluids 14, 1226 (1971).

4) Plasma Physics and Controlled Nuclear Fusion Research I. (Proc. of the 4th Int. Conf. on Plasma Phys. and Controlled Fusion Res., Madison, Wisc.,1971) IAEA, Vienna (1971) 169.

5) S. Yoshikawa,"Applications of Relativistic Electron Coils and Heating," Princeton Plasma Physics Laboratory Report TM-260, Sept. 1971.

6) D. A. Hammer and N. Rostoker, Phys. Fluids 13, 1831 (1970).

7) When the beam life times are short enough to neglect ion motion, the correct condition is $a^2 >> \lambda_E^2(1 + \Omega_e^2/\omega_e^2)$ [R. Lee and R. N. Sudan, Phys. Fluids 14, 1213 (1971)]. However, when the ion motion is included for long beam life times, the correct condition is again $a^2 >> \lambda_E^2$ provided $\Omega_i^2 << \omega_i^2$ where $\Omega_i^2 = eB_o/M_ic$ and $\omega_i^2 = 4\pi e^2 n_e/M_i$ [K. R. Chu and N. Rostoker, Laboratory of Plasma Studies Report 85, Cornell University (1971)].

8) R. V. Lovelace and R. N. Sudan, Phys. Rev. Letters 27, 1256 (1971).

9) A. A. Ivanov and L. I. Rudakov, Soviet Phys. - JETP 31, 715 (1970).

10) Ya. B. Fainberg, V. D. Shapiro, and V. I. Shevchenko, Soviet Phys. - JETP 30, 528 (1970).

11) W. E. Drummond, J. H. Malmberg, T. M. O'Neil, and J. R. Thompson, Phys. Fluids 13, 2422 (1970).

12) T. M. O'Neil, J. H. Winfrey, and J. H. Malmberg, Phys. Fluids 14, 1204 (1971).

13) R. I. Kovtun and A. A. Rukhadze, Soviet Phys. - JETP 31, 915 (1970).

14) The quoted result was $|E_M|^2/8\pi n_b \gamma_o mc^2 = 0.396$ S. However, for an electric field of the form $E = E_M(t) \cos kx$, the mean energy density is $|E_M|^2/16\pi$ instead of $|E_M|^2/8\pi$.

15) The dispersion relationship was solved without taking into account finite-size particles. The results are part of a book of dispersion relationships being compiled by the authors.

16) Here we are assuming that the growth rate of the instability is much faster than the voltage change characteristic of the diode. Typically, this voltage change is ±10% over 5-10 nanoseconds.

17) J. R. Thompson, Phys. Fluids 14, 1532 (1971).

18) I. N. Onishchenko, A. R. Linetskii, N. G. Matsiborko, V. D. Shapiro, and V. I. Shevchenko, Soviet Phys. - JETP Letters 12, 407 (1970).

19) This may also be interpreted as increased phase mixing due to relativistic effects.

20) The critical dependence is on ω/k_o and v_o since only a slight change in these quantities produces a large change in γ_W and γ_o and thus δn_b.

21) K. Nishikawa, J. Phys. Soc. Japan 24, 916, 1152 (1968).

22) J. R. Sanmartin, Phys. Fluids 13, 1533 (1970).

23) W. L. Kruer, J. M. Dawson, and R. N. Sudan, Phys. Rev. Letters 23, 838 (1969).

24) H. V. Wong, Phys. Fluids 15, 632 (1972).

25) W. L. Kruer and J. M. Dawson, Phys. Rev. Letters 25, 1174 (1970); 15, 446 (1972).

26) J. Da w s on and C. Oberman, Phys. Fluids 5, 517 (1962); 6, 394 (1964).

27) L. Thode, R. N. Sudan, S. Kainer, and J. Dawson, Bull. Am. Phys. Soc. 17, 592 (1972).

28) J. M. Dawson; C. K. Birdsall, A. B. Langdon, and H. Okuda; R. L. Morse, Chapters in Methods of Computational Physics, Vol. 9, ed. B. Alder, S. Fernbach, and M. Rotenberg (Academic Press, New York, 14850, 1969).

29) B. Rosen and W. Kruer, "Suds - A Faster Version of the Dipole Expansion," Fourth Conference on Numerical Simulation of Plasmas, proceedings, Naval Research Laboratory, Washington, D. C., 2-3 Nov. 1970.

30) H. Okuda and C. K. Birdsall, Phys. Fluids 13, 2123 (1970).

31) J. M. Dawson, Astrophysics and Space Science 13, 446 (1971).

32) Due to the use of finite-size particles the higher harmonics decay somewhat faster than they really should be.

33) S. Kainer, J. Dawson, R. Shanny, and T. Coffey, Phys. Fluids 15, 493 (1972).

34) Finite-size particles have already been taken into account in Fig. 17.

35) P. F. Byrd and M. D. Friedman, Handbook of Elliptic Integrals for Engineers and Physicists, Springer-Verlag (1954).

36) It appears that (B·16) may be slightly optimistic in light of the calculations, including electromagnetic effects, performed by H. L. Berk, "Relativistic Beam Plasma Instability in Strong Magnetic Field", Lawrence Livermore Laboratory, UCRL-73951 (1972). However, the two-stream instability is relatively insensitive to the plasma temperature whereas the cyclotron mode is expected to be reduced if the plasma temperature is taken into account.

APPENDIX A

Trapping Frequency of a Relativistic Particle in an Anharmonic Potential

Here we compute the oscillation frequency of a particle trapped by an electrostatic wave with a phase velocity close to the speed of light. In the laboratory frame the equation of motion is

$$\frac{dp'}{dt'} = qE'_o \sin (k'x'-\omega't') \qquad (A\cdot1)$$

where the prime denotes a laboratory frame quantity. Transforming to the wave frame, Eq. (A·1) becomes

$$\frac{dp}{dt} = qE_o \sin kx \quad . \qquad (A\cdot2)$$

The electric field amplitude is the same in both frames. We solve Eq. (A·2) subject to the condition that the particle has a maximum kinetic energy $(\gamma_M - 1)mc^2$ at $x = 0$ when $t = 0$.

For non-relativistic, small amplitude motion in the wave frame it is easy to see that the particle will oscillate at the bottom of the potential well with a frequency $\omega_T = (qE_o k/m)^{\frac{1}{2}}$. When transformed to the laboratory frame we have $\omega'_T = (qE_o k'/\gamma_W^3 m)^{\frac{1}{2}}$ since the wave number transforms as $k' = \gamma_W k$ and the frequency transforms as $\omega'_T = \gamma_W^{-1}\omega_T$ where $\gamma_W = (1 - (\omega'/k'c)^2)^{-\frac{1}{2}}$. Thus, in the above limit, the only change from the nonrelativistic result is that the particle has an effective mass of $\gamma_W^3 m$.

To obtain a more general solution of Eq. (A·2) we multiply by $c^{-2}dx/dt$ to obtain

$$\frac{d\gamma}{dt} = qE/mc^2 \sin kx \cdot \frac{dx}{dt} \qquad (A\cdot3)$$

where $\gamma = (1 - (c^{-1}dx/dt)^2)^{-\frac{1}{2}}$. Integrating Eq. (A·3) yields the conservation of energy condition:

$$H = \gamma mc^2 + q\phi(x) \ . \qquad (A\cdot4)$$

Here $\phi(x) = -\phi_o \cos kx$, H is the total energy, and $\phi_o = E_o/k$ is the amplitude of the potential in the wave frame. Using condition (A·4) and $\gamma = \gamma_M$ at $x = 0$ we obtain

$$\cos kx = 1 + (\gamma - \gamma_M)\, mc^2/q\phi_o \ . \qquad (A\cdot5)$$

Equation (A·3), with the aid of Eq. (A·5), can now be rewritten as

$$\frac{d\gamma}{dt} = -\frac{kc}{\gamma}\left[(2\eta - \gamma_M + \gamma)\ (\gamma_M - \gamma)\ (\gamma - 1)(\gamma + 1) \right]^{\frac{1}{2}} \qquad (A\cdot6)$$

where we have recalled the definition of the cosine and energy in terms of x(t). Here $\eta \equiv q\phi_o/mc^2$ is the ratio of the potential energy to the particle rest energy in the wave frame. Rearranging Eq. (A·6) and integrating gives

$$T = \frac{1}{kc} \int_1^{\gamma_M} \left[(\gamma + 1)\ (\gamma - 1)\ (\gamma_M - \gamma)\ (2\eta - \gamma_M + \gamma) \right]^{-\frac{1}{2}} \gamma d\gamma \qquad (A\cdot7)$$

where T is the quarter period time. For the last factor in the square root to remain positive we require $2q\phi_o > (\gamma_M - 1)\, mc^2$ which is just the condition

for the particle to remain trapped.

The integral in expression (A·7) can be performed[35] under the restrictions $\gamma_M \geq 1 > \gamma_M - 2\eta > -1$ to give

$$T = (qk^2\phi_o/m)^{-\frac{1}{2}} \left[K(h_1) + \pi\eta^{\frac{1}{2}} \left(1 - \Lambda_o(\beta_1,h_1)\right) \right] . \qquad (A\cdot8)$$

In expression (A·8), K is the elliptic integral of the first kind, $h_1^2 = \gamma_- (\gamma_+ - 2\eta)/4\eta$, $\beta_1 = \arcsin \left[2\gamma_+^{-1} \right]^{\frac{1}{2}}$, $\gamma_\pm = \gamma_M \pm 1$, and $\Lambda_o(\beta,h)$ is Heuman's Lambda Function. The above solution places an upper and lower limit on η : $0.5\gamma_- < \eta < 0.5\gamma_+$. If $\eta > 0.5\gamma_+$, then the solution of expression (A·7) can be written as

$$T = \left[(ek^2\phi_o/m)\cdot g \right]^{-\frac{1}{2}} \left[K(h_2) + \pi(\eta g)^{\frac{1}{2}} \left(1 - \Lambda_o(\beta_2,h_2)\right) \right] \qquad (A\cdot9)$$

when $\gamma_M \geq 1 > -1 > \gamma_M - 2\eta$. Here $h_2^2 = (\gamma_-/\gamma_+)\ (2\eta - \gamma_+)/(2\eta - \gamma_-)$, $\beta_2 = \arcsin \left[2\eta/(2\eta - \gamma_-) \right]^{\frac{1}{2}}$, and $g = (2\eta - \gamma_-)\gamma_+/4\eta$. For electrons oscillating in the potential well of a wave produced by the two-stream instability we expect the condition $\eta < 0.5\gamma_+$ to be satisfied except for electrons trapped close to the bottom of the well for which $\gamma_M \approx 1$ (see Eq. (19)). However, for electrons with $\gamma_M \approx 1$ both (A·8) and (A·9) give the same result of $T \approx \frac{\pi}{2} (qk^2\phi_o/m)^{-\frac{1}{2}}$. Thus we will use expression (A·8) to determine the frequency.

The total period of the oscillation is 4T. Consequently, the frequency of the oscillation is

$$\omega_T = \frac{\pi}{2} (qk^2\phi_o/m)^{\frac{1}{2}} \left(K(h_1) + \pi\eta^{\frac{1}{2}}(1 - \Lambda_o(\beta_1,h_1))\right)^{-1} . \qquad (A\cdot10)$$

At this point we note that for a nonrelativistic particle in an anharmonic potential, $\gamma_+ - 2\eta \approx 0.5(v_M/c)^2 - 2\eta$. Under these conditions $h_o^2 \approx h_1^2 \approx mv_M^2/4q\phi_o$, $\Lambda_o(\beta_1,h_1) \approx 1$, and expression (A·10) reduces to

$$\omega_T = \frac{\pi}{2}\,(ek^2\phi_o/m)^{\frac{1}{2}}/K(h_o) \qquad \text{(A·11)}$$

which is the well known solution of a particle in an anharmonic potential.

Transforming (A·10) and (A·11) to the laboratory frame we obtain

$$\omega_T' = \frac{\pi}{2}\,(qk'^2\phi_o'/m\gamma_W^3)^{\frac{1}{2}}\left(K(h_1) + \pi(q\phi_o'/\gamma_W mc^2)^{\frac{1}{2}}\cdot\left(1 - \Lambda_o(\beta_1,h_1)\right)\right)^{-1} \qquad \text{(A·12)}$$

and

$$\omega_T' = \frac{\pi}{2}\,(qk'^2\phi_o'/m\gamma_W^3)^{\frac{1}{2}}/K(h_o) \quad . \qquad \text{(A·13)}$$

For the purposes of this report we leave k_o, h_1, β_1 in terms of the wave frame quantities.

APPENDIX B

Derivation of the Maximum Linear Growth Rates for the Electron Cyclotron and Two-Stream Interactions.

The general dispersion relationship is

$$\varepsilon(\underline{k},\omega) = 1 + \mu_i(\underline{k},\omega) + \mu_e(\underline{k},\omega) + \mu_b(\underline{k},\omega)$$

where μ_α, α = i, e, b, are the susceptibilities. The electrostatic approximation yields

$$\mu_\alpha = \frac{\omega_\alpha^2}{k^2} \sum_{n=-\infty}^{n=+\infty} \int_L \int_{-\infty}^{\infty} \frac{2\pi u_\perp du_\perp du_{||}}{\omega - k_{||}v_{||} - n\Omega_\alpha\left[1+(u_\perp^2+u_{||}^2)/c^2\right]^{-\frac{1}{2}}} \left[J_n^2(k_\perp u_\perp/\Omega_\alpha) \left\{ n\Omega_\alpha \frac{\partial f_\alpha}{\partial u_\perp^2/2} + k_{||} \frac{\partial f_\alpha}{\partial u_{||}} \right\} \right] \qquad (B\cdot1)$$

In the above relationship ω_α is the plasma frequency of species α, $\Omega_\alpha \equiv eB_o/m_\alpha c$ is the cyclotron frequency ($\Omega_e = \Omega_b$), $k^2 = k_\perp^2 + k_{||}^2$, and the integration variable is $u = v(1 - v^2/c^2)^{-\frac{1}{2}}$.

We assume maxwellian distributions for the ions and electrons:

$$f_{\substack{\alpha \\ \alpha=i,e}} = (2\pi u_\alpha^2)^{-3/2} \exp(-u^2/2u_\alpha^2) .$$

Since the ion and electron thermal velocities are small compared with the speed of light, the resonance term $\omega - k_{||}v_{||} - n\Omega_\alpha\left[1+(u_\perp^2+u_{||}^2)/c^2\right]^{-\frac{1}{2}}$ can be approximated by $\omega - k_{||}v_{||} - n\Omega_\alpha$. Thus, the susceptibilities become

$$\mu_{\substack{\alpha \\ \alpha=i,e}} = \frac{\omega_\alpha^2}{k^2 v_\alpha^2} \left[1 + \frac{\omega}{\sqrt{2}\, v_\alpha k_{||}} \sum_{n=-\infty}^{n=+\infty} Z\left(\frac{\omega - n\Omega_\alpha}{\sqrt{2}k_{||}v_\alpha}\right) e^{-\lambda_\alpha} I_n(\lambda_\alpha) \right] \qquad (B\cdot2)$$

where $u_\alpha \approx v_\alpha$, and $\lambda_\alpha \equiv k_\perp^2 v_\alpha^2/\Omega_\alpha^2$. When $k_\perp v_\alpha/\Omega_\alpha \leq \cdot20$, only the n = 0, ±1

terms need to be retained in the sum. Since $v_i/c < v_e/c << 1$ we expand the plasma dispersion function, $Z(x) \approx -x^{-1}-0.5x^{-3}\ldots$where $x = \frac{\omega-n\Omega_\alpha}{\sqrt{2}\, k_{||} v_\alpha} >> 1$, to obtain

$$\mu_i = -\frac{\omega_i^2}{\omega^2}\cos^2\theta - \frac{\omega_i^2 \sin^2\theta}{\omega^2-\Omega_i^2} \qquad (B\cdot3)$$

$$\mu_e = -\frac{\omega_e^2}{\omega^2}\cos^2\theta - \frac{\omega_e^2 \sin^2\theta}{\omega^2-\Omega_e^2} \qquad (B\cdot4)$$

where $\cos\theta = k_{||}/k$. Limiting the analysis to the high frequency regime, $\omega > (\omega_e\Omega_e)^{\frac{1}{2}}$, we neglect the ion contribution. Since the beam will be considered as a small term, the main part of the dispersion relation is

$$1 - \frac{\omega_e^2}{\omega^2}\cos^2\theta - \frac{\omega_e^2 \sin^2\theta}{\omega^2-\Omega_e^2} \approx 0. \qquad (B\cdot5)$$

Solving (B·5) for ω^2 we obtain

$$\omega^2 = \frac{1}{2}\Omega_e^2\,(1+\omega_e^2/\Omega_e^2)\left[1 \pm \left(1 - \frac{4\omega_e^2\cos^2\theta}{\Omega_e^2(1+\omega_e^2/\Omega_e^2)}\right)^{\frac{1}{2}}\right] \qquad (B\cdot6)$$

where $\omega_e/\Omega_e << 1$. To order $(\omega_e/\Omega_e)^2$, the two roots of (B·6) are:

$$\omega_+^2 = \Omega_e^2(1+\omega_e^2/\Omega_e^2\sin^2\theta)$$

and $\qquad (B\cdot7)$

$$\omega_-^2 = \omega_e^2\cos^2\theta \,.$$

For the beam, the resonance term in (B·1) couples the $u_\perp$ and $u_{||}$ inte-

gration. To simplify the resonance term we make the two mass approximation and choose

$$f_b = \delta(u_o - u_{||}) \ (2\pi u_{\perp,b}^2)^{-1} \exp(-u_\perp^2/2u_{\perp,b}^2)$$

where $u_{\perp,b} = \gamma_o v_{\perp,b}$ and $\gamma_o = (1+u_o^2/c^2)^{\frac{1}{2}}$. For $k_\perp v_{\perp,b}/\Omega_R \lesssim .20$, the beam susceptibility can be written as

$$\mu_b = -\frac{\omega_{b\perp}^2 \sin^2\theta}{(\omega - k_{||}v_o)^2 - \Omega_R^2} - \frac{\omega_{b||}^2 \cos^2\theta}{(\omega - k_{||}v_o)^2} \qquad (B\cdot 8)$$

where $\Omega_R \equiv \Omega_e/\gamma_o$, $\omega_{b\perp}^2 = \omega_b^2/\gamma_o$, and $\omega_{b||}^2 = \omega_b^2/\gamma_o^3$.

To find the maximum growth rates we set $\omega = \omega_\pm + \delta\omega$ where $\delta\omega/\omega_\pm \ll 1$ and ω_+ and ω_- are given by (B·7). Expanding (B·5) about $\omega = \omega_\pm$ we obtain

$$1 + \mu_e \approx \delta\omega \cdot \frac{\partial \mu_e}{\partial \omega}\bigg|_{\omega_\pm} = \frac{2\cdot\delta\omega}{\omega_\pm}\left[\frac{\omega_e^2}{\omega_\pm^2}\cos^2\theta + \frac{\frac{\omega_\pm}{\omega_e}\sin^2\theta}{\left[\frac{\omega_\pm^2}{\omega_e^2} - \frac{\Omega_e^2}{\omega_e^2}\right]^2}\right].$$

Examining (B·8), there are three possible cases which may produce an unstable root:

i) $\omega_\pm \approx kv_o \cos\theta$,

ii) $\omega_\pm \approx kv_o \cos\theta + \Omega_e/\gamma_o$,

and

iii) $\omega_\pm \approx kv_o \cos\theta - \Omega_e/\gamma_o$.

Case (i) (Two-Stream)

a) $\omega_+ \approx kv_o \cos\theta$ and $\omega = \omega_+ + \delta\omega$

$$1 + \mu_e + \mu_b \approx \frac{2\cdot\delta\omega}{\omega_e}(\Omega_e/\omega_e)^3 \sin^{-2}\theta - \frac{\omega_{b||}^2 \cos^2\theta}{(\delta\omega)^2} = 0$$

$$\omega/\omega_e = (\Omega_e/\omega_e)\cdot\omega_+ - \frac{1}{2\gamma_o}\,(n_b/2n_e)^{1/3}\,(\omega_e/\Omega_e)^{1/3}\cos^{2/3}\theta\,\sin^{2/3}\theta$$

$$\delta/\omega_e = \frac{\sqrt{3}}{2}\,\frac{1}{\gamma_o}\,(n_b/2n_e)^{1/3}\,(\omega_e/\Omega_e)^{1/3}\cos^{2/3}\theta\,\sin^{2/3}\theta \qquad (B\cdot9)$$

b) $\omega_- = kv_o\cos\theta$ and $\omega = \omega_- + \delta\omega$

$$1 + \mu_e + \mu_b \approx \frac{2\cdot\delta\omega}{\omega_e\cos\theta} - \frac{\omega_{b\parallel}^2\cos^2\theta}{(\delta\omega)^2} = 0$$

$$\omega/\omega_e = \cos\theta - \frac{1}{2\gamma_o}\,(n_b/2n_e)^{1/3}\cos\theta$$

$$\delta/\omega_e = \frac{3}{2\gamma_o}\,(n_b/2n_e)^{1/3}\cos\theta \qquad (B\cdot10)$$

Case (ii) (Cyclotron - Normal Doppler Effect)

a) $\omega_+ \approx kv_o\cos\theta + \Omega_e/\gamma_o$ and $\omega = \omega_+ + \delta\omega$

$$1 + \mu_e + \mu_b \approx \frac{2\cdot\delta\omega}{\omega_+}\,(\Omega_e/\omega_e)^2\sin^{-2}\theta - \frac{\omega_{b\perp}^2\sin^2\theta}{2\Omega_R\cdot\delta\omega} = 0$$

$$\omega/\omega_e = (\Omega_e/\omega_e)\cdot\omega_+ \pm \frac{1}{2}\,(n_b/n_e)^{1/2}\,(\omega_e/\Omega_e)\sin^2\theta$$

$$\delta/\omega_e = 0 \qquad (B\cdot11)$$

b) $\omega_- \approx kv_o\cos\theta + \Omega_e/\gamma_o$ and $\omega \approx \omega_- + \delta\omega$

$$1 + \mu_e + \mu_b \approx \frac{2\cdot\delta\omega}{\omega_e\cos\theta} - \frac{\omega_{b\perp}^2\sin^2\theta}{2\Omega_R\cdot\delta\omega} = 0$$

$$\omega/\omega_e = \cos\Theta \pm \frac{1}{2}(n_b/n_e)^{1/3}(\Omega_e/\omega_e)^{1/2}\sin\Theta\cos^{1/2}\Theta$$

$$\delta/\omega_e = 0 \qquad \text{(B·12)}$$

Case (iii) (Cyclotron - Anomolous Doppler Effect)

a) $\omega_+ \approx kv_o\cos\Theta - \Omega_e/\gamma_o$ and $\omega = \omega_+ + \delta\omega$

$$1 + \mu_e + \mu_b \approx \frac{2\cdot\delta\omega}{\omega_+}(\Omega_e/\omega_e)^2\sin^{-2}\Theta + \frac{\omega_{b\perp}^2\sin^2\Theta}{2\Omega_R\cdot\delta\omega} = 0$$

$$\omega/\omega_e = (\Omega_e/\omega_e)\cdot\omega_+ + \frac{1}{2}(n_b/n_e)^{1/2}(\omega_e/\Omega_e)\sin^2\Theta$$

$$\delta/\omega_e = \frac{1}{2}(n_b/n_e)^{1/2}(\omega_e/\Omega_e)\sin^2\Theta \qquad \text{(B·13)}$$

b) $\omega_- \approx kv_o\cos\Theta - \Omega_e/\gamma_o$ and $\omega = \omega_- + \delta\omega$

$$1 + \mu_e + \mu_b \approx \frac{2\cdot\delta\omega}{\omega_e\cos\Theta} + \frac{\omega_{b\perp}^2\sin^2\Theta}{2\Omega_R\cdot\delta\omega} = 0$$

$$\omega/\omega_e = \cos\Theta + \frac{1}{2}(n_b/n_e)^{1/2}(\omega_e/\Omega_e)^{1/2}\sin\Theta\cos^{1/2}\Theta$$

$$\delta/\omega_e = \frac{1}{2}(n_b/n_e)^{1/2}(\omega_e/\Omega_e)^{1/2}\sin\Theta\cos^{1/2}\Theta \qquad \text{(B·14)}$$

In order to obtain (B·9) through (B·14) we have assumed that $\Omega_e^2/\omega_e^2 >> 1$. For sake of argument, we will choose $\Omega_e^2/\omega_e^2 \approx 10$ which appears to satisfy the approximations used provided γ_o is not too large. Under the above conditions, the three largest growth rates are:

$$\text{a)}\quad \delta_o^-/\omega_e = \frac{\sqrt{3}}{2^{4/3}}\,\frac{1}{\gamma_o}\,(\omega_b/\omega_e)^{2/3} \qquad \text{at} \quad \cos\Theta = 1 \tag{B·10'}$$

$$\text{b)}\quad \delta_o^+/\omega_e = \frac{\sqrt{3}}{4}\,\frac{1}{\gamma_o}\,(\omega_b/\omega_e)^{2/3}\,(\omega_e/\Omega_e)^{1/3} \quad \text{at} \cos\Theta = \frac{1}{\sqrt{2}} \tag{B·9'}$$

$$\text{c)}\quad \delta_{-1}^-/\omega_e = \frac{1}{2}\,(\tfrac{2}{9})^{1/4}\,(\omega_b/\omega_e)\,(\omega_e/\Omega_e)^{1/2} \quad \text{at} \quad \cos\Theta = \frac{1}{\sqrt{3}} \tag{B·14'}$$

The superscript $\pm$ refers to $\omega \approx \omega_\pm$ and the subscript $_{-1}^{o}$ refers to the resonance at $n = {}_{-1}^{o}$. Now, in order to approximate the unstable spectrum by a one-dimensional model, we require

$$\text{a)}\ \delta_o^-/\delta_o^+ > 2$$

and (B·15)

$$\text{b)}\ \delta_o^-/\delta_{-1}^- > 2 \quad .$$

Since we expect the two-stream instability to e-fold approximately 7-10 times, this will insure that over 95% of the energy lost by the beam is due to the two-stream instability. Substituting (B·10'), (B·11), and (B·14') into (B·15) we obtain $\Omega_e/\omega_e \gtrsim 2$ from (a) and $\Omega_e/\omega_e \gtrsim 1.26\ \gamma_o^{\,2}(n_b/2n_e)^{1/3} \approx \gamma_o S$ from (b). Therefore, the requirement for a one-dimensional spectrum reduces to[36]

$$\Omega_e^{\,2}/\omega_e^{\,2} \gtrsim 10 \qquad \text{and} \qquad \Omega_e/\omega_e \gtrsim \gamma_o S \quad . \tag{B·16}$$

APPENDIX C

Proof of Energy Transfer Relationship

Here we show that

$$2\gamma\beta_W \cdot \Delta\beta_W \leq S(1+S)^{-\frac{1}{2}} \qquad (C\cdot1)$$

where $\beta_W = \beta_o(1-0.5\gamma_o^{-1}(n_b/2n_e)^{1/3})$, $\Delta\beta_W = \Delta v_W/c = 0.5\beta_o\gamma_o^{-1}(n_b/2n_e)^{1/3}\cdot(1-\beta_o\beta_W)^{-1}$, and $\gamma = (1-(\Delta\beta_W)^2)^{-\frac{1}{2}}$. Using the expression for $\beta_W, \Delta\beta_W$ and γ can be expressed as

$$\Delta\beta_W = 0.5\beta_o^{-1}S(1 + 0.5S)^{-1} \qquad (C\cdot2)$$

and

$$\gamma = (1 + 0.5S)(1 + S - 0.25S^2\gamma_o^{-2}\beta_o^{-2})^{-\frac{1}{2}} . \qquad (C\cdot3)$$

The left hand side of (C·1) can then be rewritten as

$$2\gamma\beta_W \cdot \Delta\beta_W = S(1+S)^{-\frac{1}{2}}\left[\frac{(1 - 0.5S\gamma_o^{-2}\beta_o^{-2})}{(1 - 0.25\gamma_o^{-2}\beta_o^{-2}S^2(1+S)^{-1})^{\frac{1}{2}}}\right] \qquad (C\cdot4)$$

Now in the limit $\gamma_o >> 1$ (i.e. for a given value of n_b/n_e, $\Delta\beta_W$ increases as γ_o increases) $0.25\gamma_o^{-2}\beta_o^{-2}S^2(1+S)^{-1} \to 0.25(n_b/2n_e)^{2/3}(1+S)^{-1} << 1$ and thus we may expand the square root for all S since as $\gamma_o \to 1$, $0.25\gamma_o^{-2}\beta_o^{-2}S^2(1+S)^{-1} \to 0$. Therefore,

$$2\gamma\beta_W \cdot \Delta\beta_W \approx S(1+S)^{-\frac{1}{2}}\left[1 - \frac{0.5}{\gamma_o^2\beta_o^2}\left\{S - 0.25S^2(1+S)^{-1}\right\}\right] \qquad (C\cdot5)$$

where $S - 0.25S^2(1+S)^{-1} \geq 0$ for $S \geq 0$.

In the limit $\gamma_o >> S >> 1$

$$2\gamma\beta_W \cdot \Delta\beta_W \to S(1+S)^{-\frac{1}{2}}\left[1 - \frac{0.375}{\gamma_o}(n_b/2n_e)^{1/3}\right] \approx S(1+S)^{-\frac{1}{2}} \qquad (C\cdot6)$$

and in the limit $\gamma_o \to 1$

$$2\gamma\beta_W \cdot \Delta\beta_W \rightarrow S(1+S)^{-\frac{1}{2}} \left[1 - 0.5(n_b/2n_e)^{1/3} \right] < S(1+S)^{-\frac{1}{2}} \qquad (C\cdot7)$$

Consequently,

$$2\gamma\Delta\beta_W \cdot \beta_W \leq S(1+S)^{-\frac{1}{2}} \quad \text{for all } S. \qquad (C\cdot8)$$

The exact relationship $2\gamma\beta_W \Delta\beta_W$ was compared to $S(1+S)^{-\frac{1}{2}}$ for $n_b/n_e = 1/9$ and $\gamma_o = 1$ to $\gamma_o = 16$. The maximum error (for $n_b/n_e < 1/9$ the error is smaller) was found to be 6% in the range $S = 0.3$ to $S = 0.6$.

TABLE and FIGURE CAPTIONS

Table 1: Summary of the eleven computer simulations performed. Columns (1)-(7) give the basic parameters for each run. The system length is denoted by L, and the number of simulation particles used are N_e (electrons$\cdot 10^{-3}$), N_i (ions$\cdot 10^{-3}$), and N_b (beam electrons$\cdot 10^{-3}$). The initial plasma electron temperature (T_e) is given in column (8) in units of kev. Columns (9) and (10) are the maximum theoretical growth rates ($\delta^T_{k_o}/\omega_e = 0.866\gamma_o^{-1}(n_b/2n_e)^{1/3}$) and the maximum growth rates from the simulations. The maximum growth rates obtained from the numerical solution of Eq. (8), corrected for finite-size particles, are given in parentheses. The strength parameter ($S \equiv \beta_o^2\gamma_o(n_b/2n_e)^{1/3}$) is given in column (11). In column (12) the percentage of total electric field energy in the dominant mode is given. The maximum fraction of initial beam energy converted into electric field energy as a result of the hydrodynamic two-stream instability ($W \equiv \sum_k |E_k|^2/8\pi n_b\gamma_o mc^2$) is given in column (13). For the nonrelativistic runs (R1) and (R2), $W = \sum_k |E_k|^2/4\pi n_b m v_o^2$. N is the number of times the two-stream instability e-folded and $R = 10^{-2}\omega_E^2/\omega_e^2 = 10^{-2}\, n_b/\gamma_W^3 n_e$ is the effective beam to plasma frequency ratio. These are given in columns (14) and (15). Finally, the fraction of kinetic energy lost by the beam after the completion of the second stage (K) is given in column (16).

Figure 1: Numerical solution of Eq. (8) for the frequency ω_k and growth rate δ_k as a function of wave number when $\gamma_o = 4$ and $n_b/n_e = 0.01$.

Figure 2a: Laboratory frame sketch of phase space at time $t = t_o$. Initially

the beam electrons move over a single wave with relative velocity $\Delta v_W/c = 0.5\gamma_o^{-1}(n_b/2n_e)^{1/3}(1 - \omega v_o/k_o c^2)^{-1}$. The solid line represents the separatrix of a fixed potential $\phi(t_o)$. The initial beam momentum is p_o and $p_W = m\gamma_W\omega/k_o$.

Figure 2b: Laboratory frame sketch of phase space at time $t = t_1$. Trapping begins when the separatrix passes through the actual beam trajectory. The shaded line segment represents trapped beam electrons.

Figure 2c: Laboratory frame sketch of phase space at time $t = t_2$. Wave saturation occurs when the beam electrons trapped at $t = t_1$ have rotated one-half revolution in phase space (i.e. from point Q_1 to point Q_2). The intermediate dashed lines represent the orbits trapped electrons, electrons trapped between $t = t_1$ and $t = t_2$, would have if the potential was fixed at $\phi(t_2)$.

Figure 3 : Sketch of the logarithm of the electric field energy in the dominant mode $(\ell n|E_{k_o}|^2/16\pi)$ as a function of time.

Figure 4: The separatrix in the wave frame is plotted for various values of $\Delta v_W/c$. As $\Delta v_W/c$ increases the separatrix becomes more peaked. Only the positive segment ($p/mc > 0$) of the separatrix is plotted.

Figure 5a: The momentum distribution assumed in the determination of δn_b .

Figure 5b: The velocity intervals about ω/k and v_o assumed in the determination of δn_b . Recall that $\Delta v/2\Delta v_o$ was taken to be unity.

Figure 6: Laboratory frame orbits an electron would follow if it moved according to $(\gamma-1)mc^2 + e\phi_o \cos kx = H$ in the wave frame. In this case, $e\phi_o/mc^2 = 0.50$, $\gamma_W = 4.0$, and H is given for each orbit.

Figure 7: Observed growth rates as a function of wave number for (R4) compared

to the numerical solution of Eq. (8), with (solid line) and without (dashed line) the finite-size of the simulation particles taken into account.

Figure 8: $|E_{k_o}|^2/16\pi n_b\gamma_o mc^2$, $T_e = \frac{1}{2}mv_{e_o}{}^2{}_{r.m.s.}$, $T_i = \frac{1}{2}M_i v_{i,r.m.s.}^2$, and $\langle v\rangle_e^2$ for (R4) plotted as a function of time. Here we are only interested in showing that the above quantities all grow at the same rate and thus the vertical axis is not specifically scaled.

Figure 9: $|E_m|^2/16\pi n_b\gamma_o mc^2$ plotted as a function of the mode number (m) for (R7) shortly before the time of saturation of the fundamental mode (m = 14). In this case the wave length of mode m is given by $\lambda_m = 85.5\lambda_E/m$ with $\lambda_{14} = 6.10\lambda_E$.

Figure 10: Harmonic electric field energy ($|E_n|^2/16\pi n_b\gamma_o mc^2$) plotted as a function of the spatial harmonic number (n) for (R7), (R4), and (R11). The power law dependence is of the form $|E_{k=nk_o}|^2 = |E_{k_o}|^2 n^\alpha$.

Figure 11: The maximum fraction of initial beam energy converted into electric field energy during the hydrodynamic two-stream instability ($W \equiv \sum_k |E_k|^2/8\pi n_b\gamma_o mc^2$) as a function of the strength parameter ($S \equiv \beta_o{}^2\gamma_o(n_b/2n_e)^{1/3}$). The dashed line is Eq. (1) and the solid line is Eq. (4).

Figure 12: Momentum distribution of the beam electrons for (R11) shortly after wave saturation. The group of electrons with $p/mc \approx 3.0$ to 3.4 correspond to electrons trapped at $t = t_1$ in Fig. 2b. The distribution is normalized to unity $\int f_b dp = 1$.

Figure 13a: Segment of phase space near the time of wave saturation for (R2). This is a nonrelativistic check run in which electron acceleration

is quite evident with $\omega_E^2/\omega_e^2 = 0.05$. The system length is $L = 3.42\lambda_E$. In Figs. 13a,b and 14a,b the beam electrons are represented by the circles and the plasma electrons by the dots.

Figure 13b: Segment of phase space near the time of wave saturation for (R4). In this case $\omega_E^2/\omega_e^2 = 0.0315$. The system length is $L = 76.2\lambda_E$.

Figure 14a: Segment of phase space near the time of wave saturation for (R7). Here $\omega_E^2/\omega_e^2 = 0.0322 \times 10^{-2} << 0.038$ and electron acceleration does not appear to have significantly affected the level of wave saturation. The system length is $L = 85.5\lambda_E$.

Figure 14b: Segment of phase space near the time of wave saturation for (R11). Here $\omega_E^2/\omega_e^2 = 0.049 \times 10^{-2} << 0.038$ and the system length is $L = 44.0\lambda_E$.

Figure 15: Comparison of the oscillation frequencies in wave amplitude and the trapping frequency associated with the bottom of the potential well. Here $\eta = e\phi_M/\gamma_w mc^2$ is the ratio of potential energy to electron rest energy in the wave frame, ϕ_M is the laboratory frame potential, and the curve is $\gamma_w^2\omega_T/\omega_e = \eta^{1/2}$.

Figure 16: Ln $|E_{k_o}|^2/16\pi n_b\gamma_o mc^2$ and ion density fluctuations $\sum_k |n_k|^2/|n_o|^2$ are plotted as a function of time for (R7). The increase in ion density fluctuations is coincident with the beginning of wave decay.

Figure 17: Segments of electron and ion phase space for (R7) at $\omega_e t = 900$. Electrons are being accelerated out of both sides of the distribution and large ion fluctuations are present.

Figure 18: Ion fluctuation growth rates as a function of wave number for (R9).

The curve is the oscillating two-stream growth rate as a function of wave number predicted by Eq. (22) with $x = 2.0$, $\mu = 1/2000$, and $\omega_o = 0.959\omega_e$.

Figure 19: Time evolution of the electron velocity distribution for (R8). Time $\omega_e t = 180$ is the end of the first stage. Time $\omega_e t = 600$ is the end of the second stage during which anomalous heating produces a heavily populated, energetic tail on both sides of the distribution.

Figure 20: Total electric field energy ($\sum_k |E_k|^2/8\pi n_b \gamma_o mc^2$) as a function of time for (R8). The stages of heating are indicated as well as the period of oscillation in wave amplitude. In this run 94% of the electric field energy was in the dominant mode at $\omega_e t = 180$.

Figure 21: Typical combined plasma and beam electron velocity distribution at the beginning of the third stage. The distribution also has a large negative tail which is not shown. The distributions are normalized to $\int f_e(v)dv = 1$ and $\int f_b(v)dv = n_b/n_e$. The run is (R8).

Figure 22: The average electron kinetic energy is given as a function of time. Here ① and ② denote the end of the first and second stages.

Figure 23: The energy corresponding to the average root mean square velocity ($0.5mv^2_{r.m.s.}$) in units of kev is given as a function of time. The magnitude of the energy is substantially lower than in Fig. 22. Time $\omega_e t = 0$ indicates the beginning of the instability and not necessarily the run.

Run #	(1) γ_o	(2) n_b/n_e	(3) M_i/m	(4) $L\omega_e/c$	(5) N_e	(6) N_i	(7) N_b	(8) T_e	(9) $\delta^T_{k_o}/\omega_e$	(10) $\delta^S_{k_o}/\omega_e$	(11) S	(12) %	(13) W	(14) N	(15) R	(16) K
1	1	.004	2000	8.2	18	20	2	10^{-3}	0.109	0.097	---	--	0.138	---	0.40	---
2	1	.05	2000	3.42	18	20	2	10^{-3}	0.253	0.245	---	--	0.223	---	5.00	---
3	2	.05	2000	38.2	9	10	1	1.5	0.117	0.115	0.435	54	0.0685	6.3	1.08	0.25
4	2	.1125	2000	76.2	9	10	1	10^{-3}	0.151	0.149	0.555	50	0.0615	9.7	3.15	0.26
5	4	.001	500	171.0	9	10	1	10^{-3}	0.0170 (0.0151)	0.145	0.296	72	0.0460	7.0	0.0023	0.30
6	4	.001	2000	171.0	9	10	1	10^{-3}	0.0170 (0.0157)	0.154	0.296	74	0.0485	7.1	0.0023	0.29
7	4	.01	2000	85.5	9	10	1	10^{-3}	0.0362	0.0358	0.617	97	0.0910	7.1	0.032	0.26
8	4	.01	2000	85.5	18	20	2	1.5	0.0362	0.0360	0.617	94	0.0845	6.5	0.032	0.29
9	4	.05	2000	42.7	9	10	1	1.5	0.0587 (0.0572)	0.0565	1.15	93	0.0650	5.5	0.0022	0.26
10	8	.01	2000	87.3	18	20	2	1.5	0.0183	0.0175	1.31	93	0.0720	5.6	0.0069	0.31
11	8	.05	2000	44.0	9	10	1	1.5	0.0310	0.0304	2.32	90	0.0515	7.0	0.049	0.27

TABLE 1

FIGURE 1

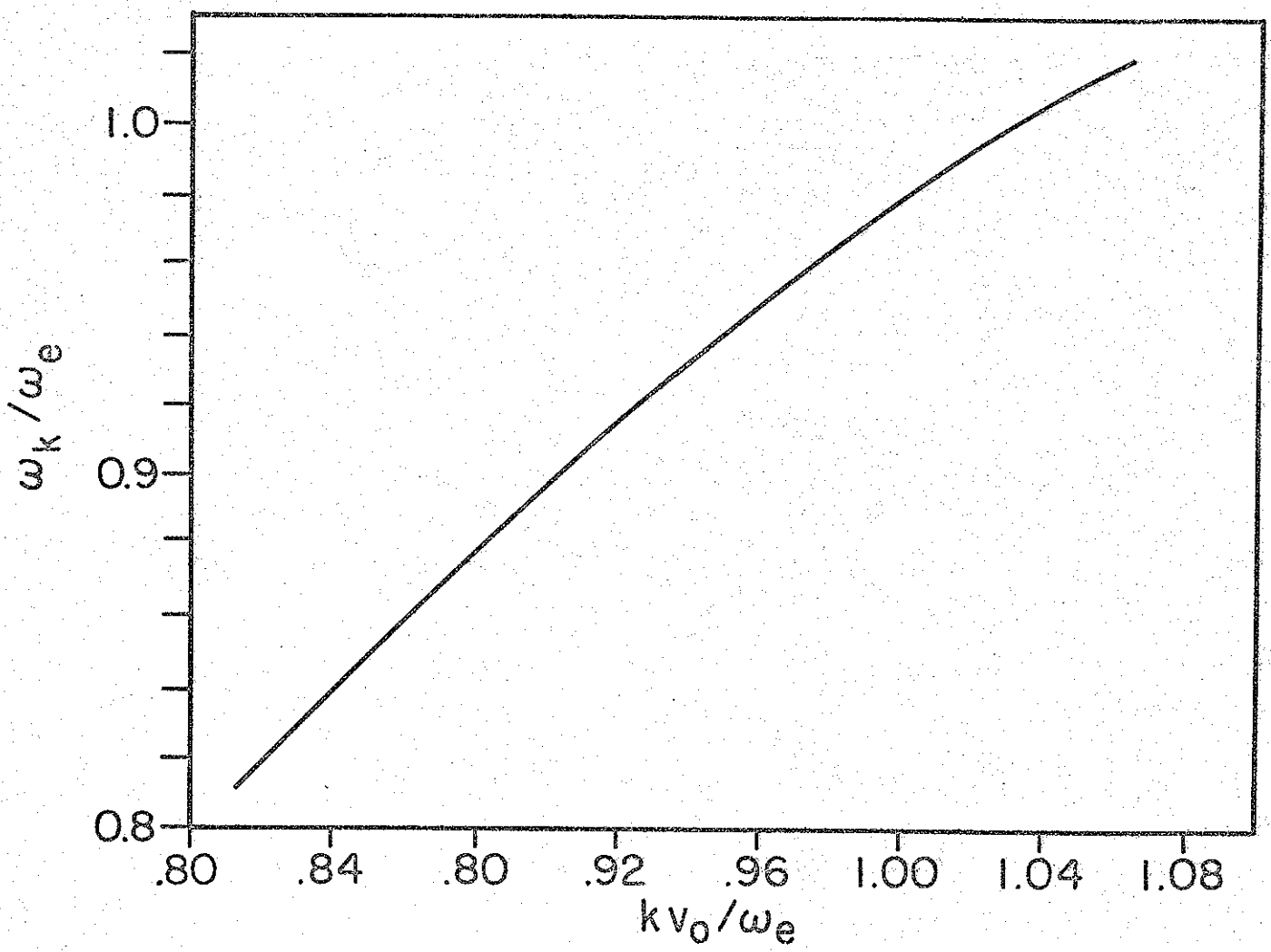
1.0
0.9
0.8
ω_k/ω_e
.80
.84
.80
.92
.96
1.00
1.04
1.08
kv_0/ω_e

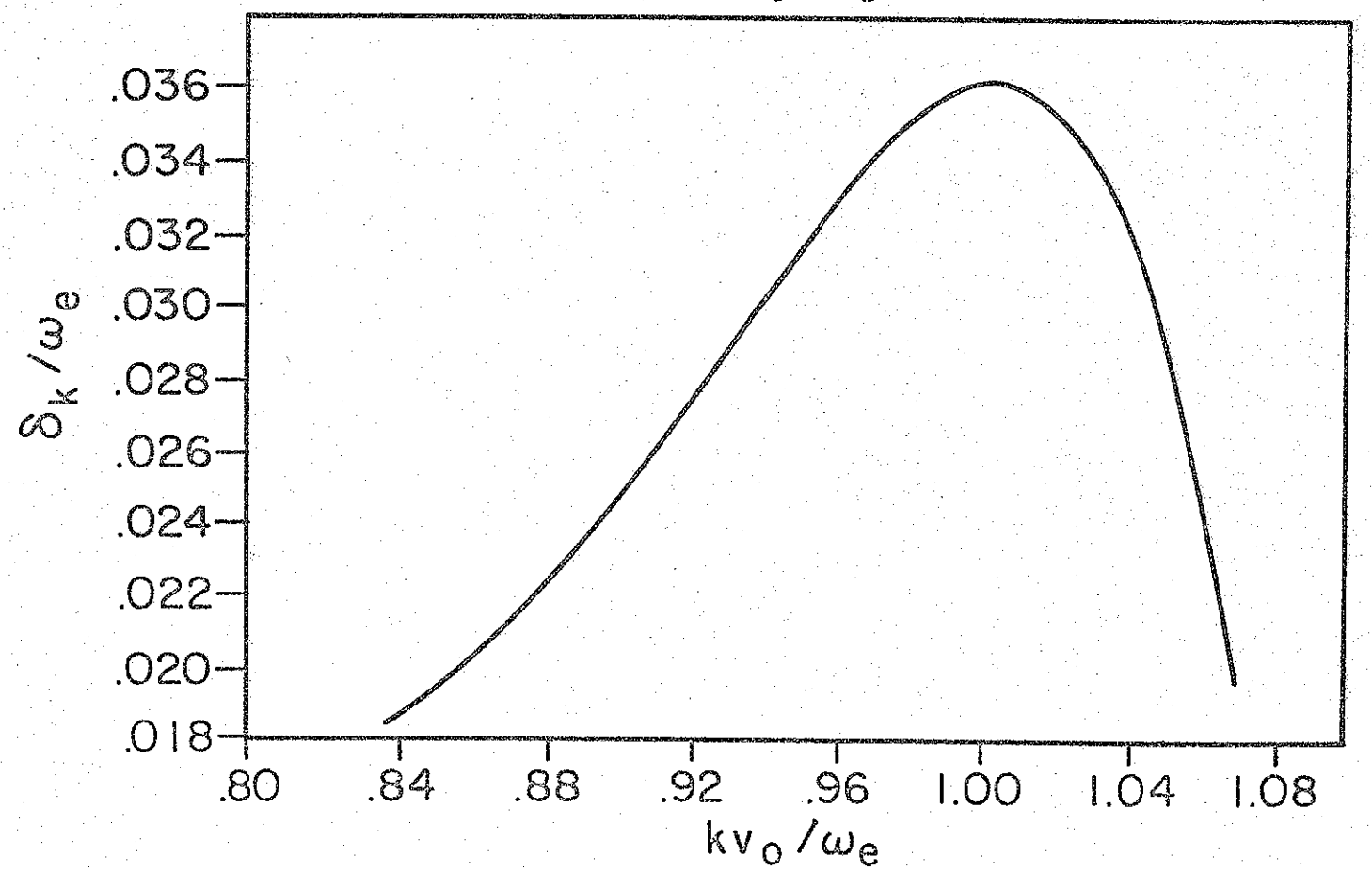
.036
.034
.032
.030
.028
.026
.024
.022
.020
.018
δ_k/ω_e
.80
.84
.88
.92
.96
1.00
1.04
1.08
kv_0/ω_e

Fig. 2a

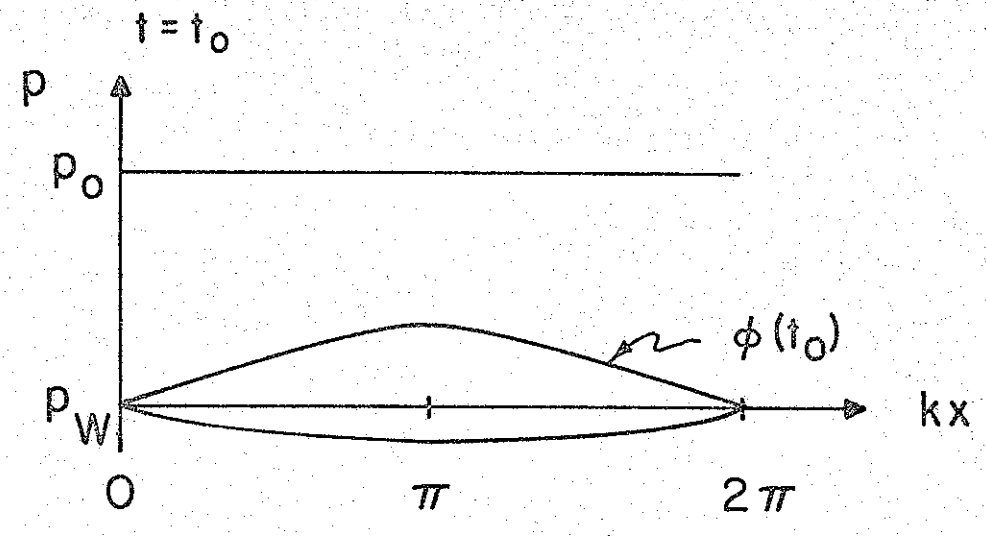

Fig. 2b

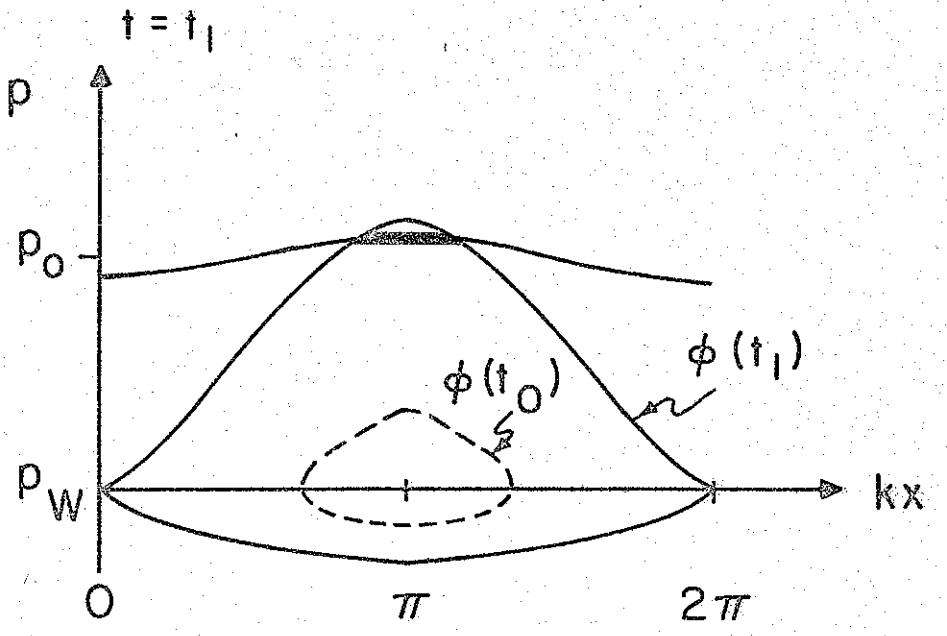

Fig. 2c

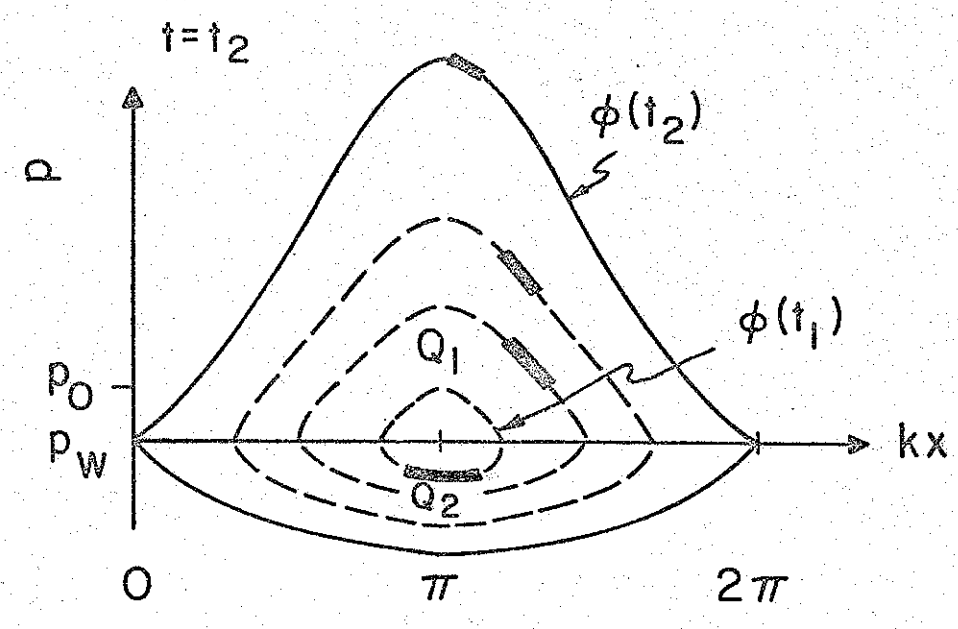

Fig. 3

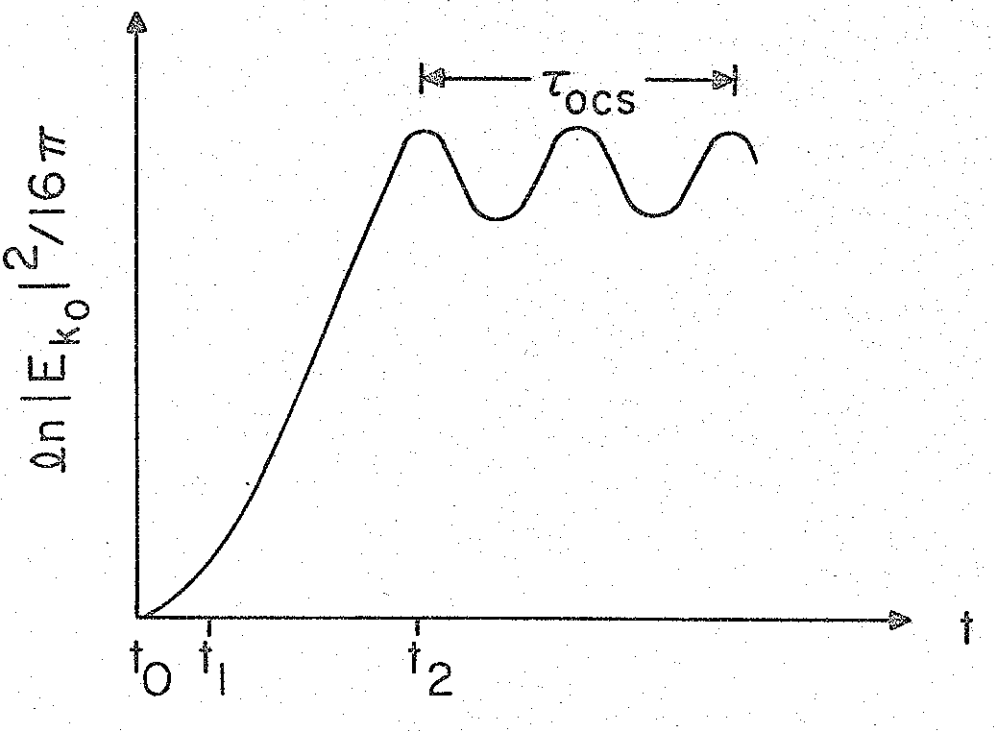

FIGURE 4

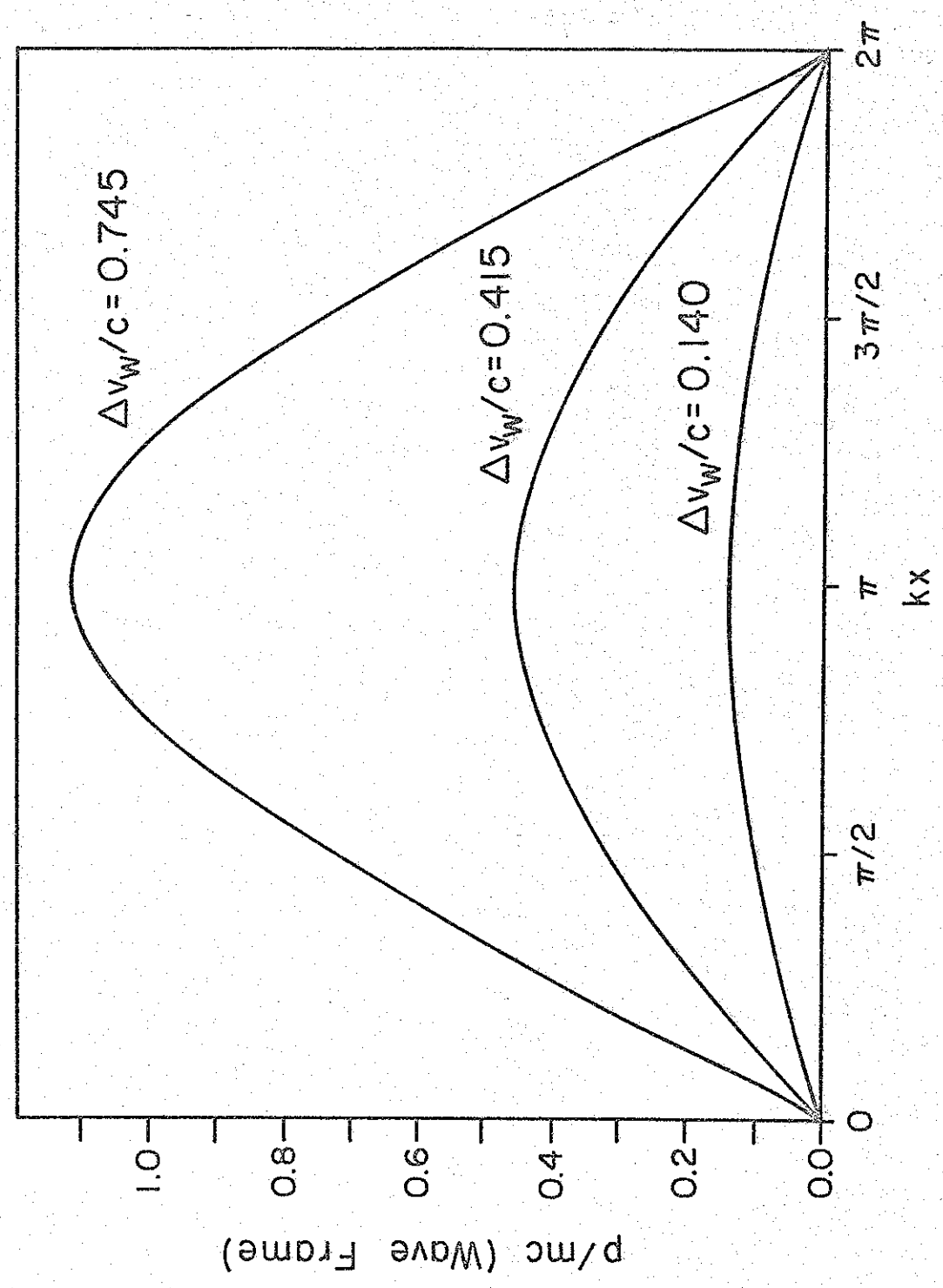
$\Delta v_w/c = 0.745$
$\Delta v_w/c = 0.415$
$\Delta v_w/c = 0.140$
0.0
0.2
0.4
0.6
0.8
1.0
p/mc (Wave Frame)
0
π/2
π
3π/2
2π
kx

FIGURE 5a

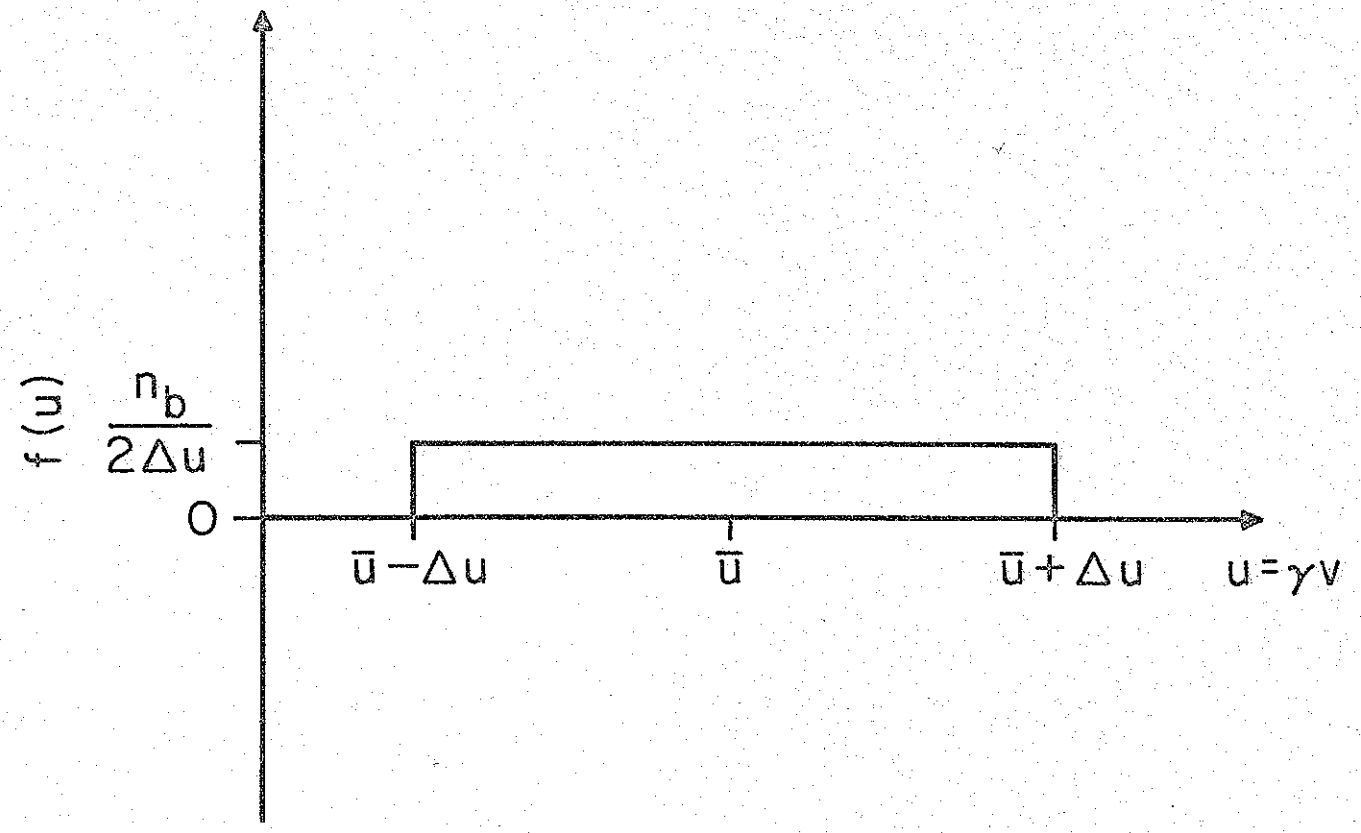

FIGURE 5b

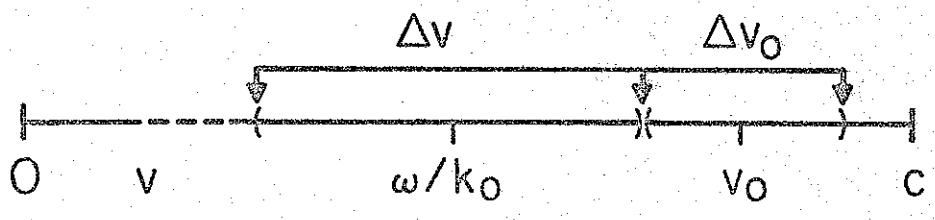

FIGURE 6

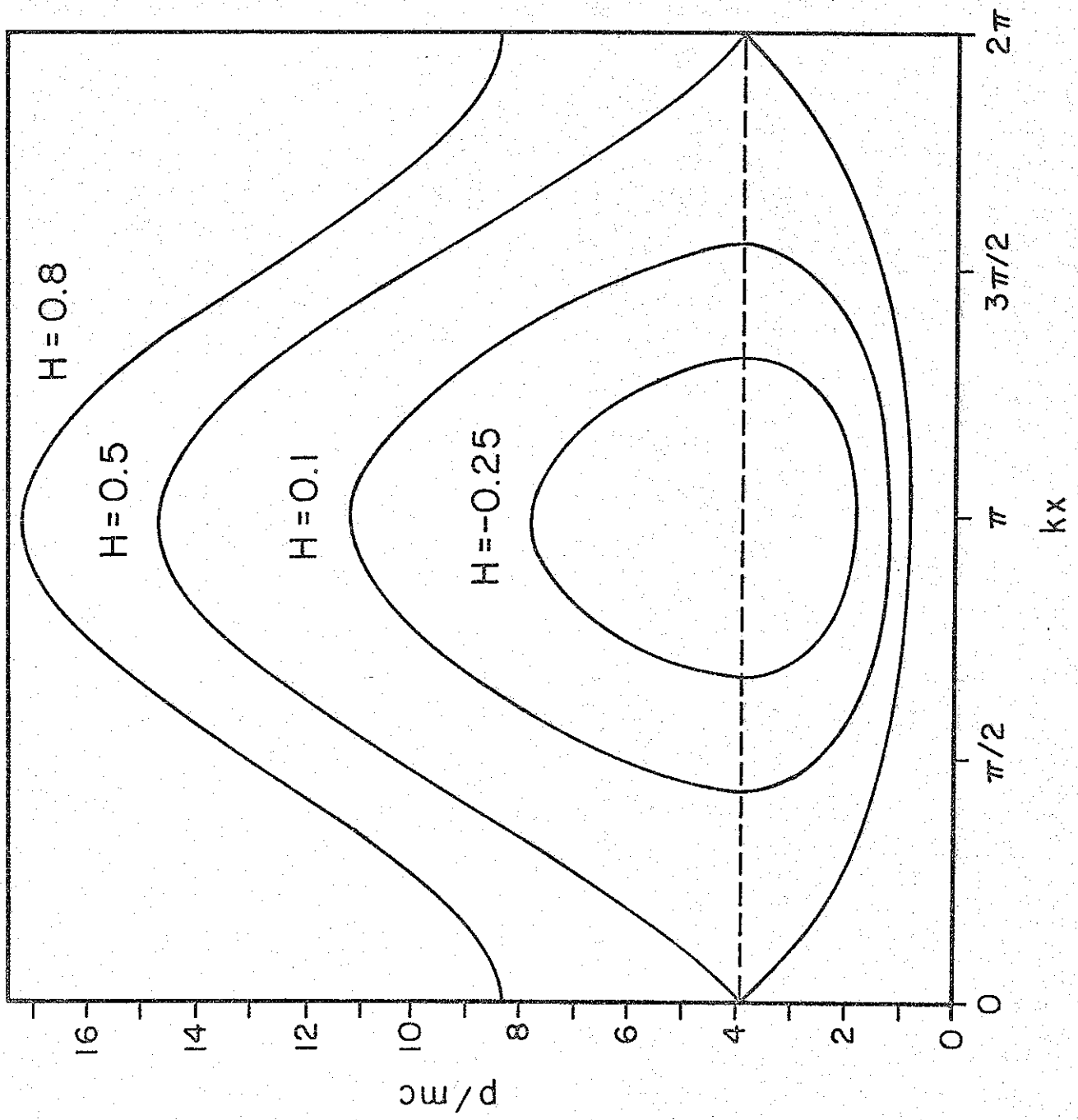

FIGURE 7

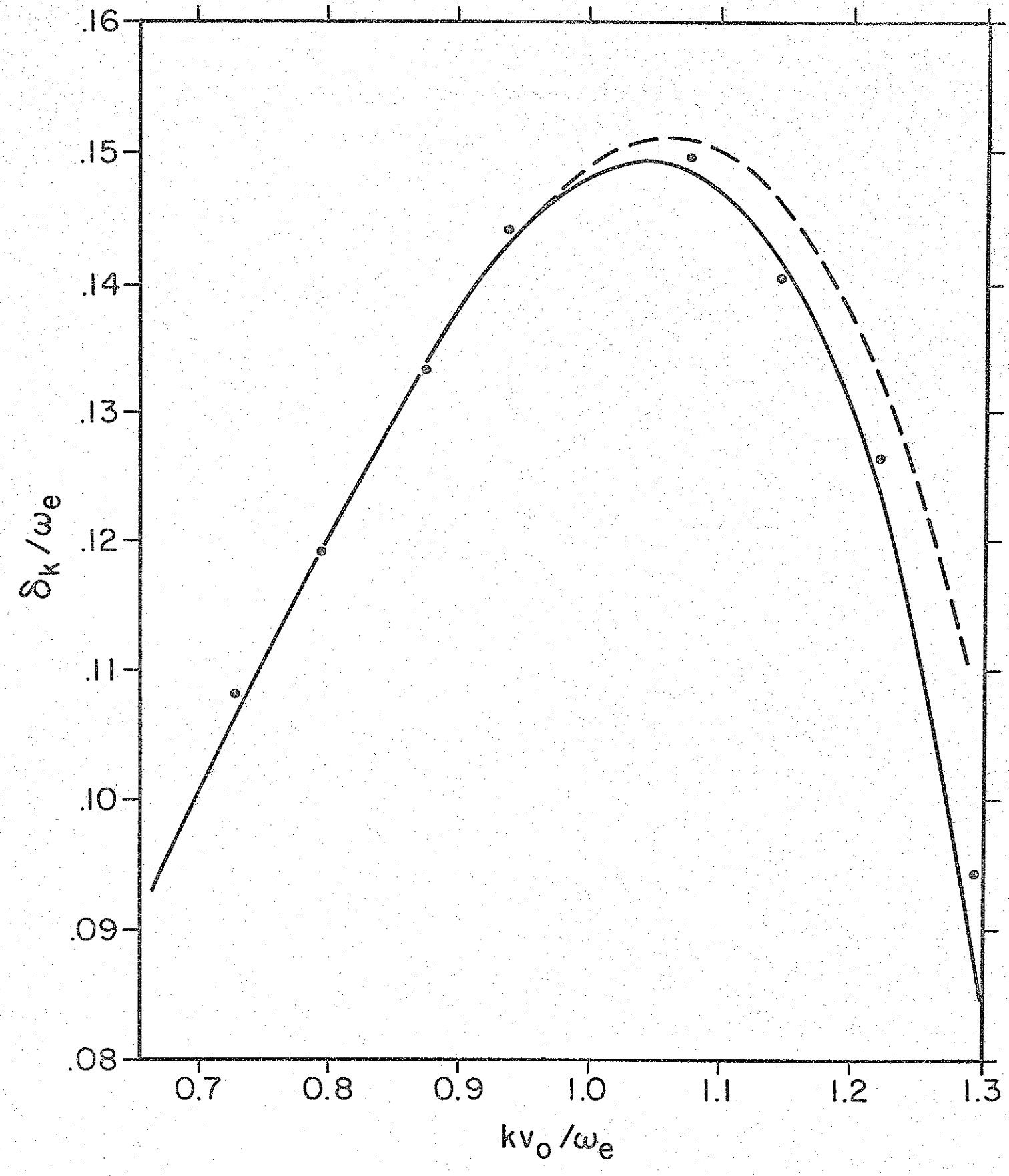
.16
.15
.14
.13
.12
.11
.10
.09
.08
δ_k / ω_e
0.7
0.8
0.9
1.0
1.1
1.2
1.3
kv_0 / ω_e

FIGURE 8

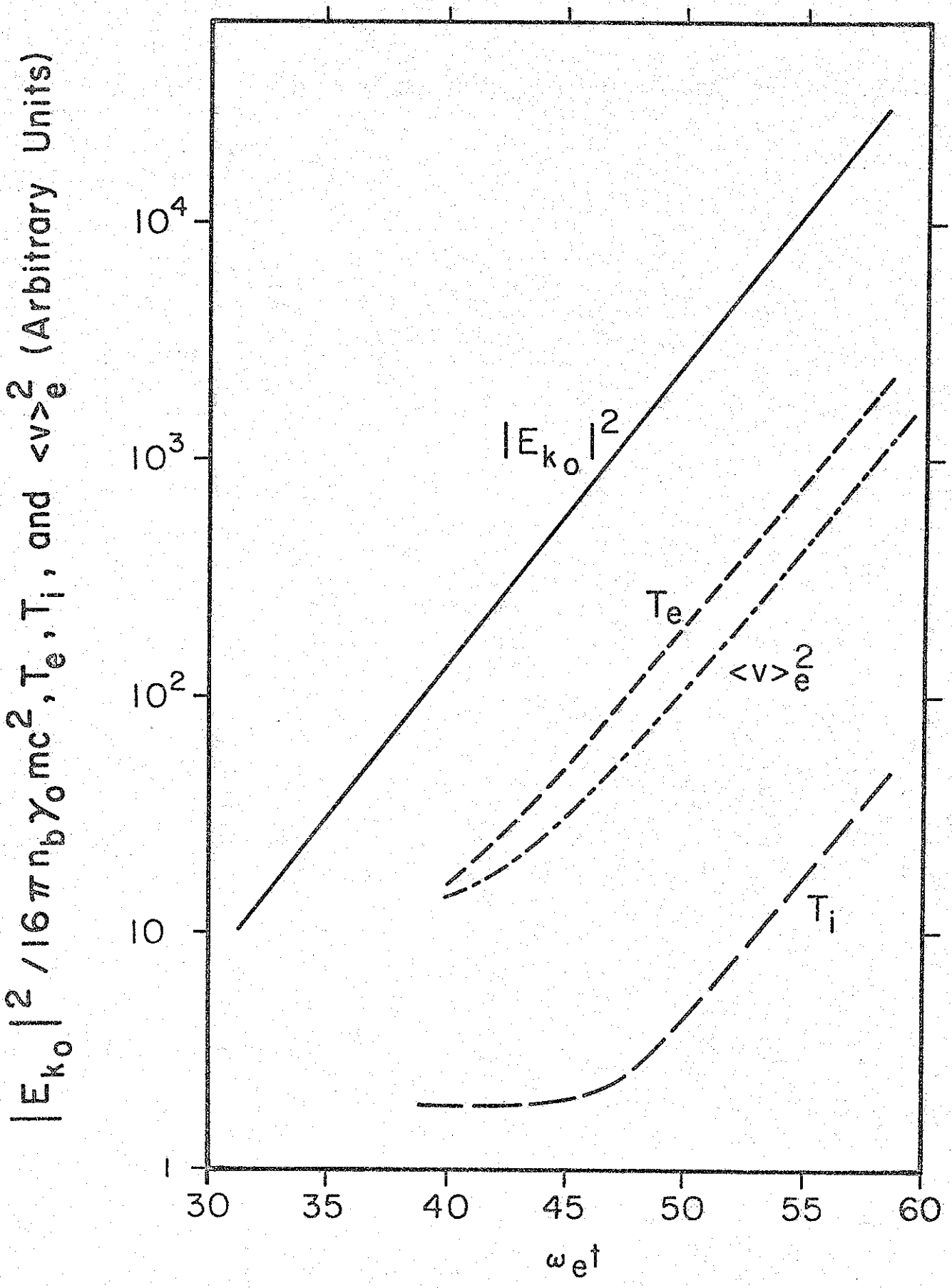
$|E_{k_o}|^2/16\pi n_b \gamma_o mc^2, T_e, T_i$, and $\langle v\rangle_e^2$ (Arbitrary Units)
10^4
10^3
10^2
10
1
30
35
40
45
50
55
60
$\omega_e t$
$|E_{k_o}|^2$
T_e
$\langle v\rangle_e^2$
T_i

FIGURE 9

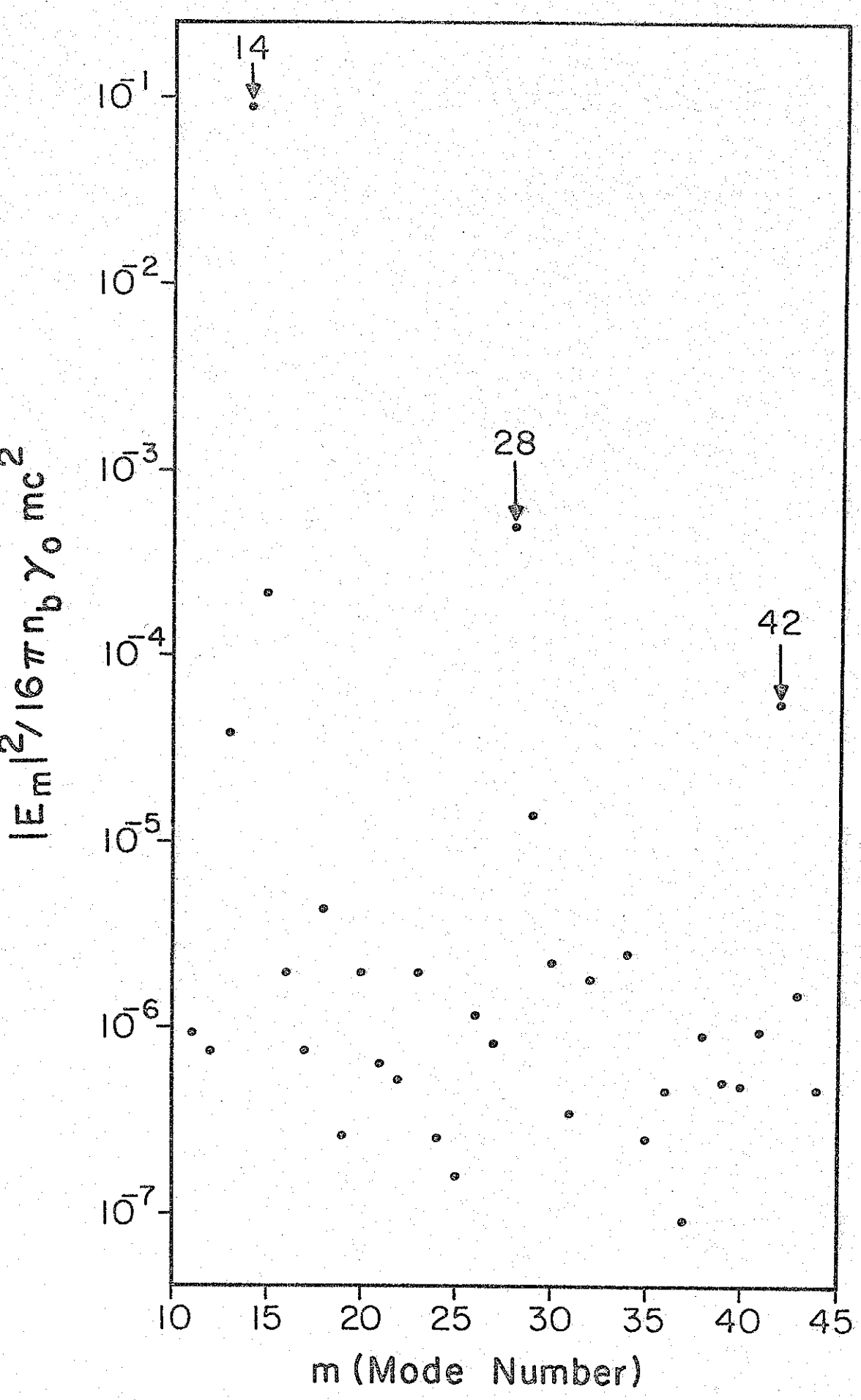
14
28
42
10^{-1}
10^{-2}
10^{-3}
10^{-4}
10^{-5}
10^{-6}
10^{-7}
$|E_m|^2/16\pi n_b \gamma_o mc^2$
10
15
20
25
30
35
40
45
m (Mode Number)

FIGURE 10

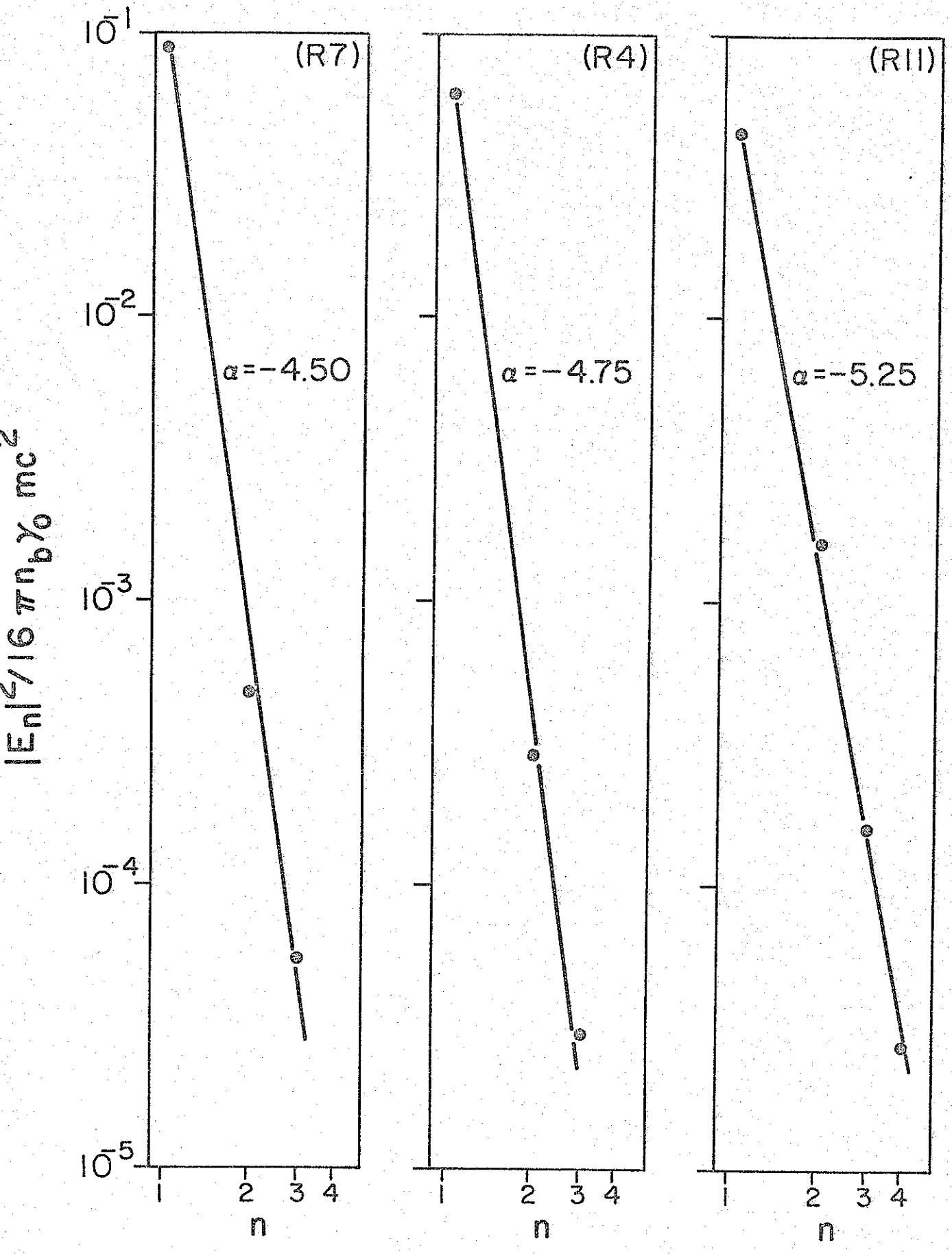
(R7)
(R4)
(R11)
α=−4.50
α=−4.75
α=−5.25
10^{-1}
10^{-2}
10^{-3}
10^{-4}
10^{-5}
$|E_n|^2/16\pi n_b \gamma_0 mc^2$
1
2
3
4
n

FIGURE II

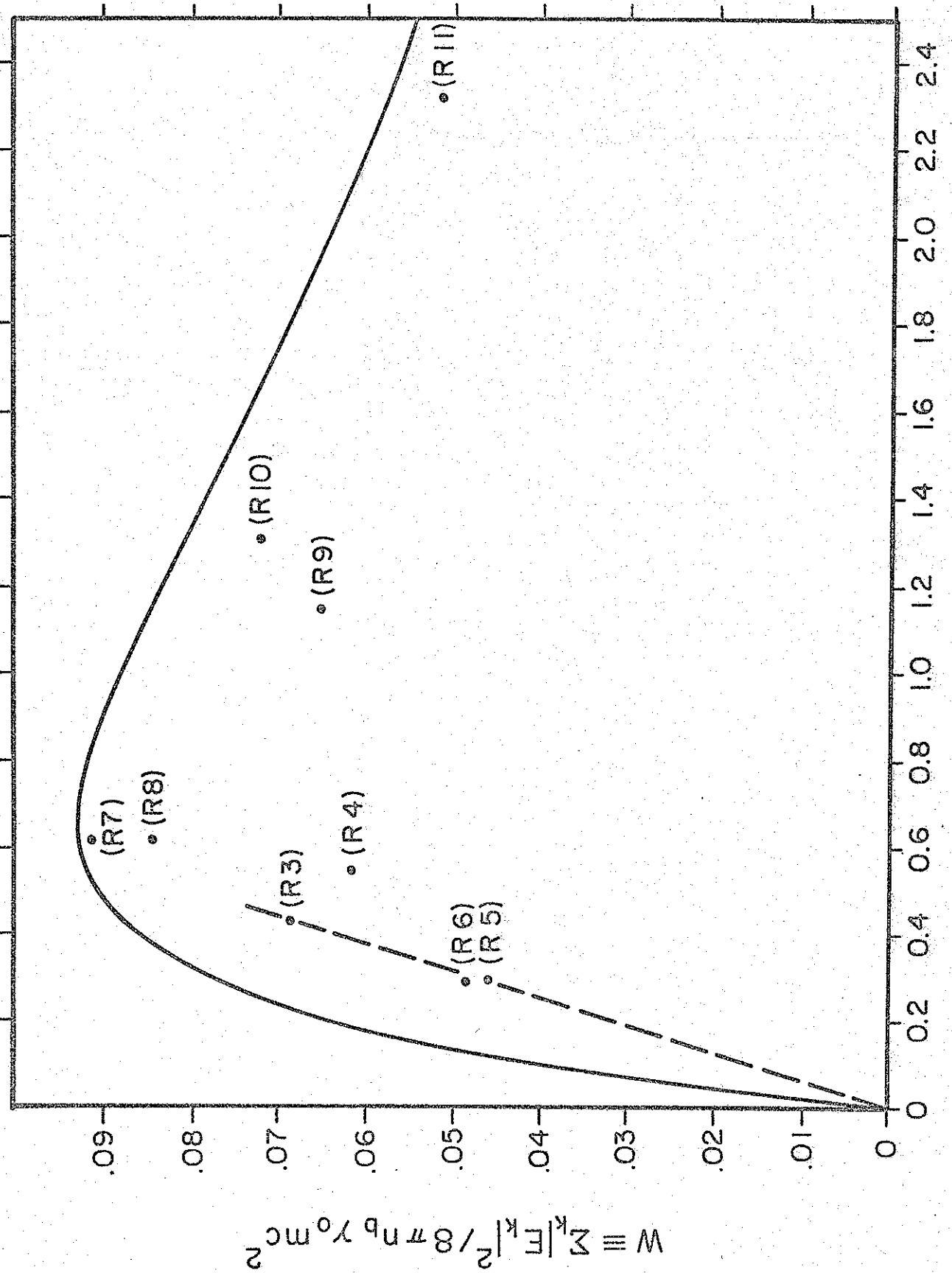
$W \equiv \Sigma_k |E_k|^2 / 8\pi n_b \gamma_o mc^2$
0
.01
.02
.03
.04
.05
.06
.07
.08
.09
0
0.2
0.4
0.6
0.8
1.0
1.2
1.4
1.6
1.8
2.0
2.2
2.4
$S = \beta_o^2 \gamma_o (n_b / 2 n_e)^{1/3}$
(R11)
(R10)
(R9)
(R8)
(R7)
(R4)
(R3)
(R6)
(R5)

FIGURE 12

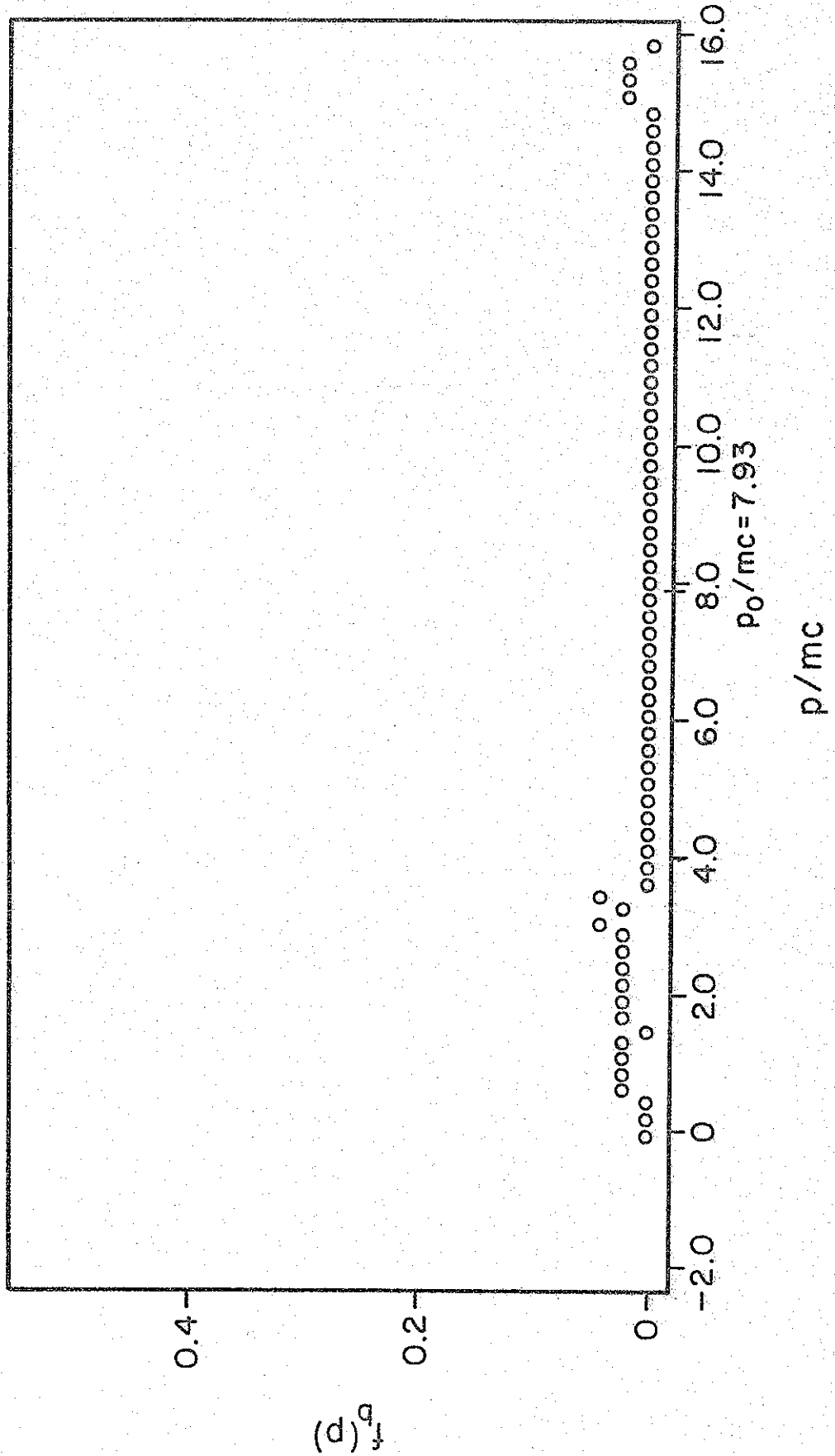

FIGURE 13a

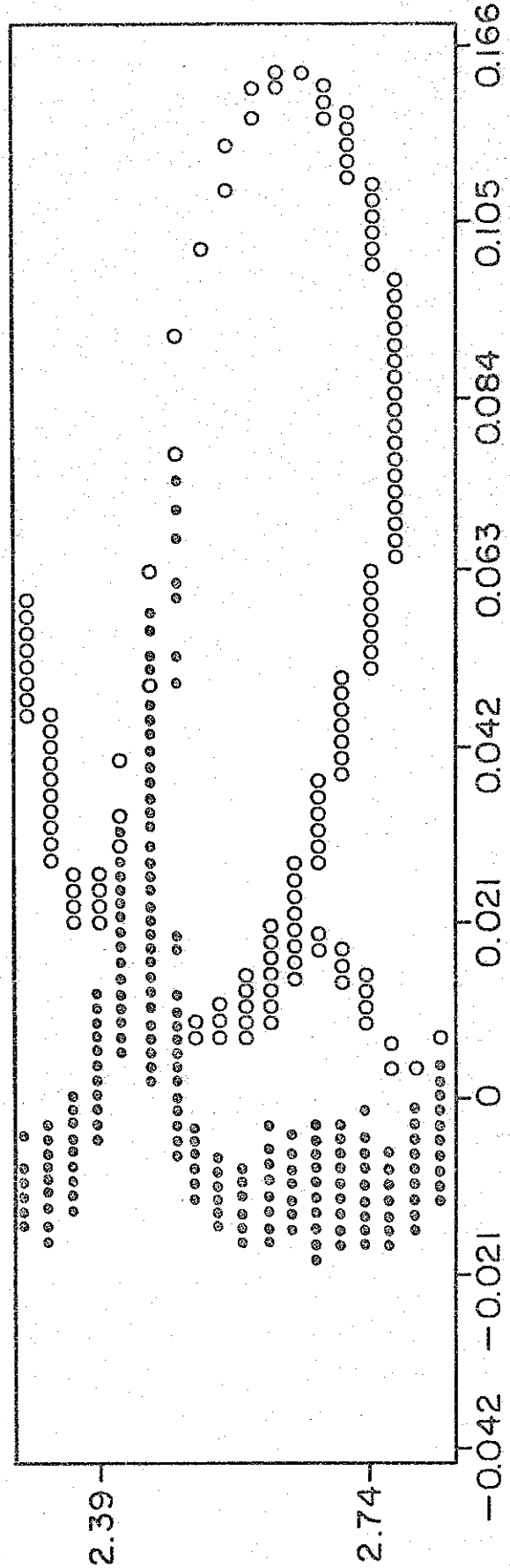

FIGURE 13b

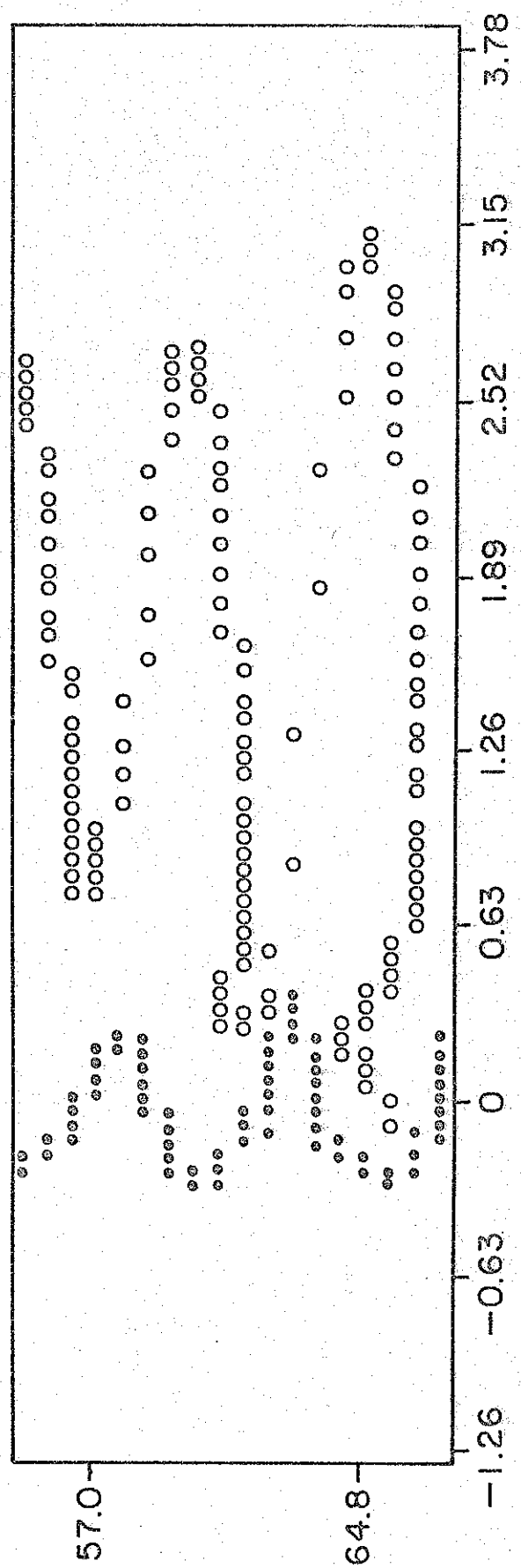

FIGURE 14a

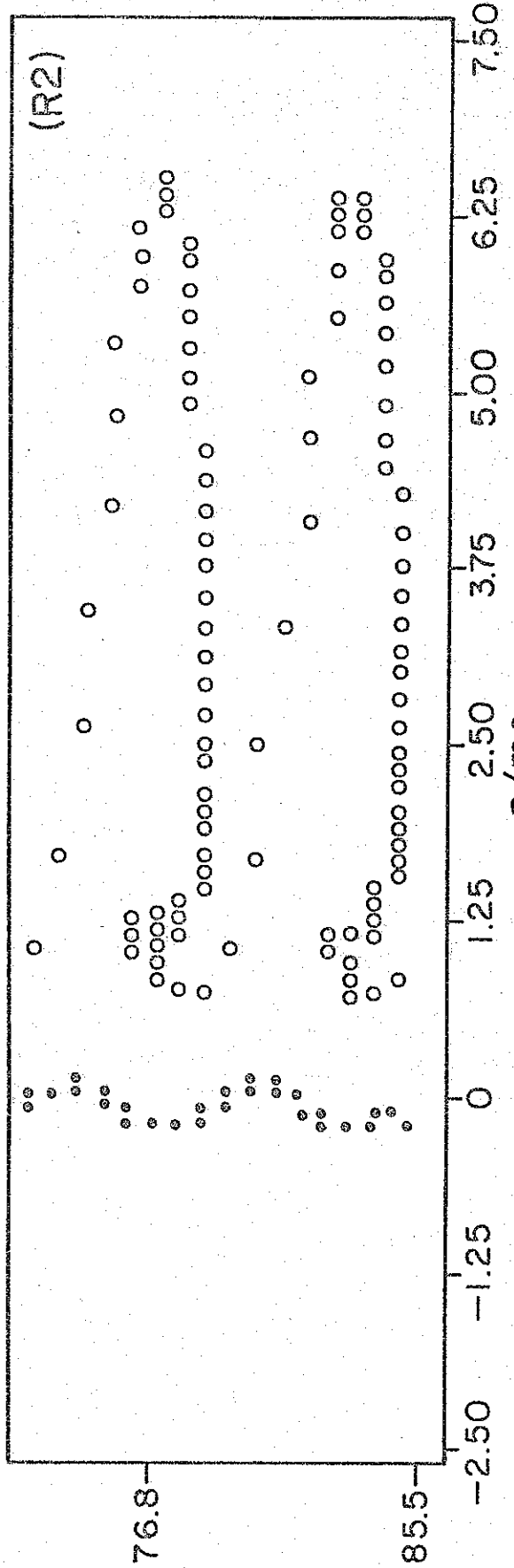

FIGURE 14b

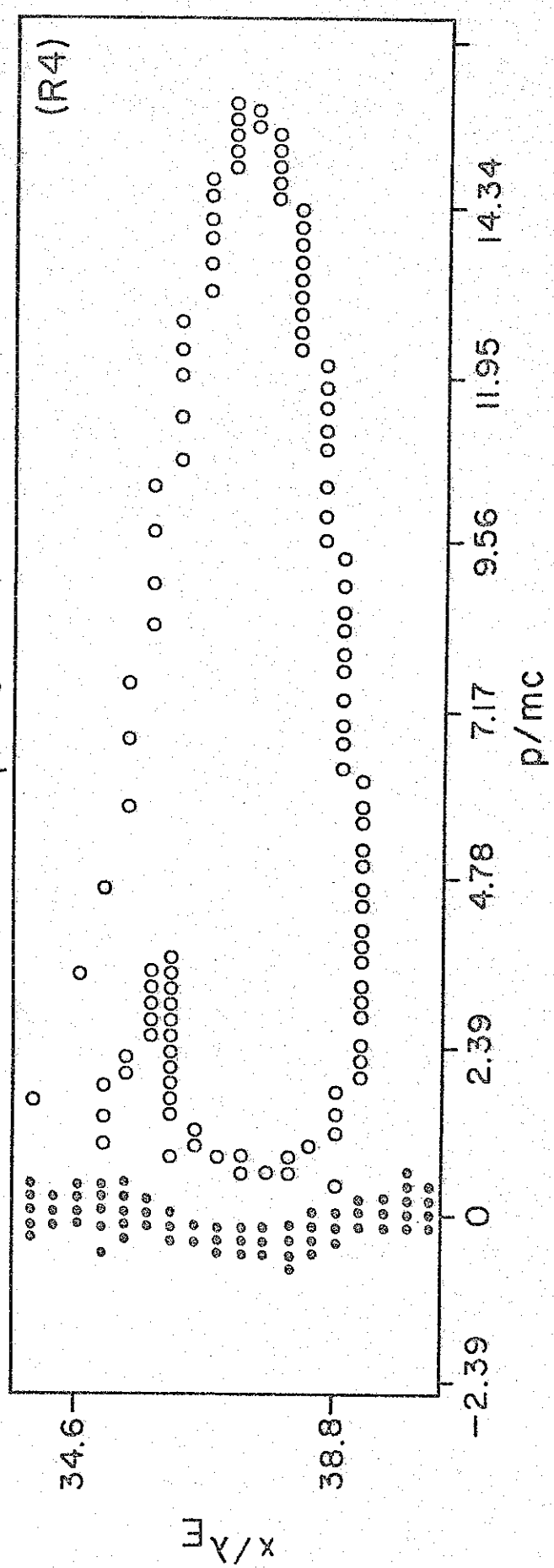

FIGURE 15

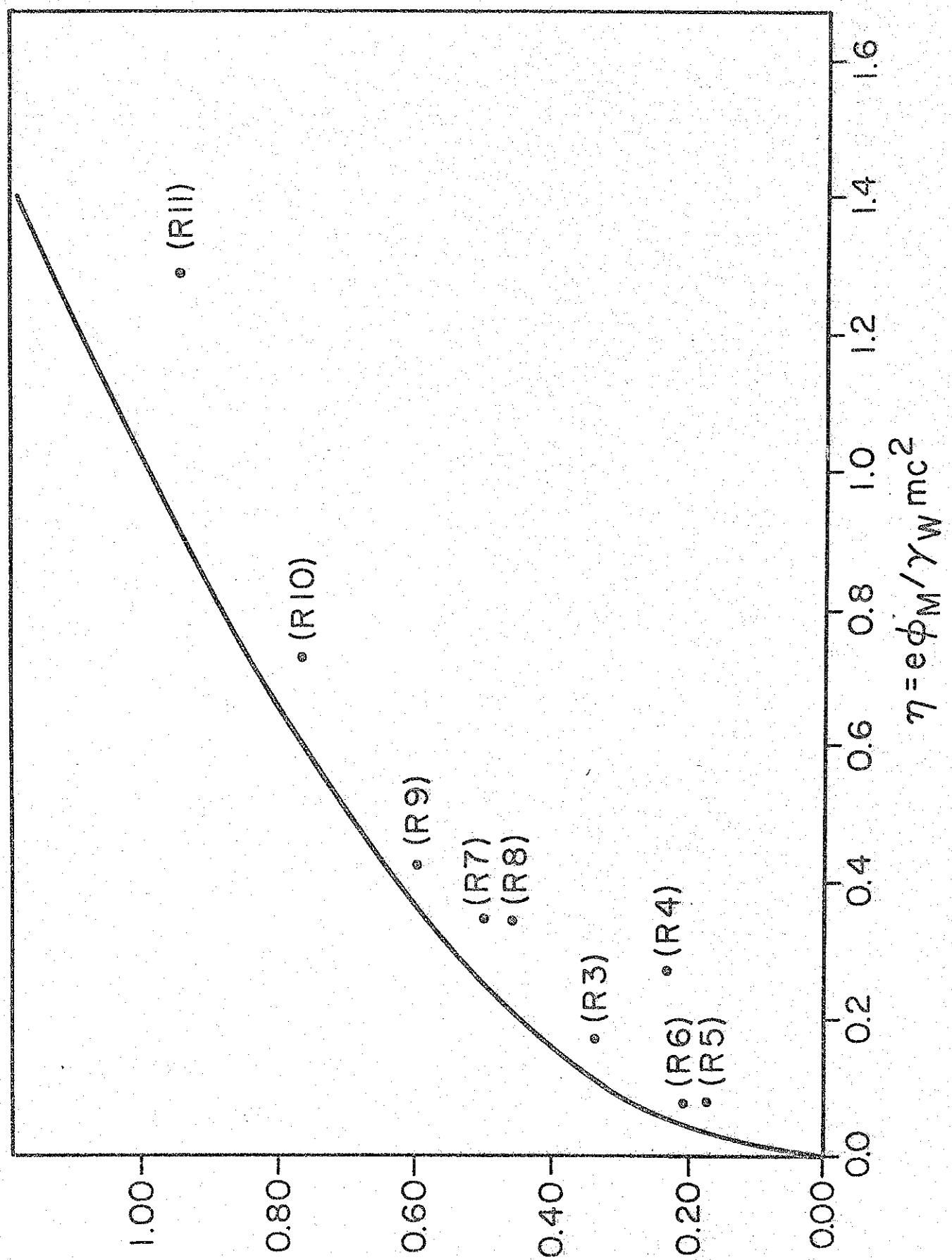
(R11)
(R10)
(R9)
(R7)
(R8)
(R3)
(R4)
(R6)
(R5)
0.00
0.20
0.40
0.60
0.80
1.00
0.0
0.2
0.4
0.6
0.8
1.0
1.2
1.4
1.6
$\gamma_W^2 \omega_T / \omega_e$
$\eta = e\phi_M / \gamma_W mc^2$

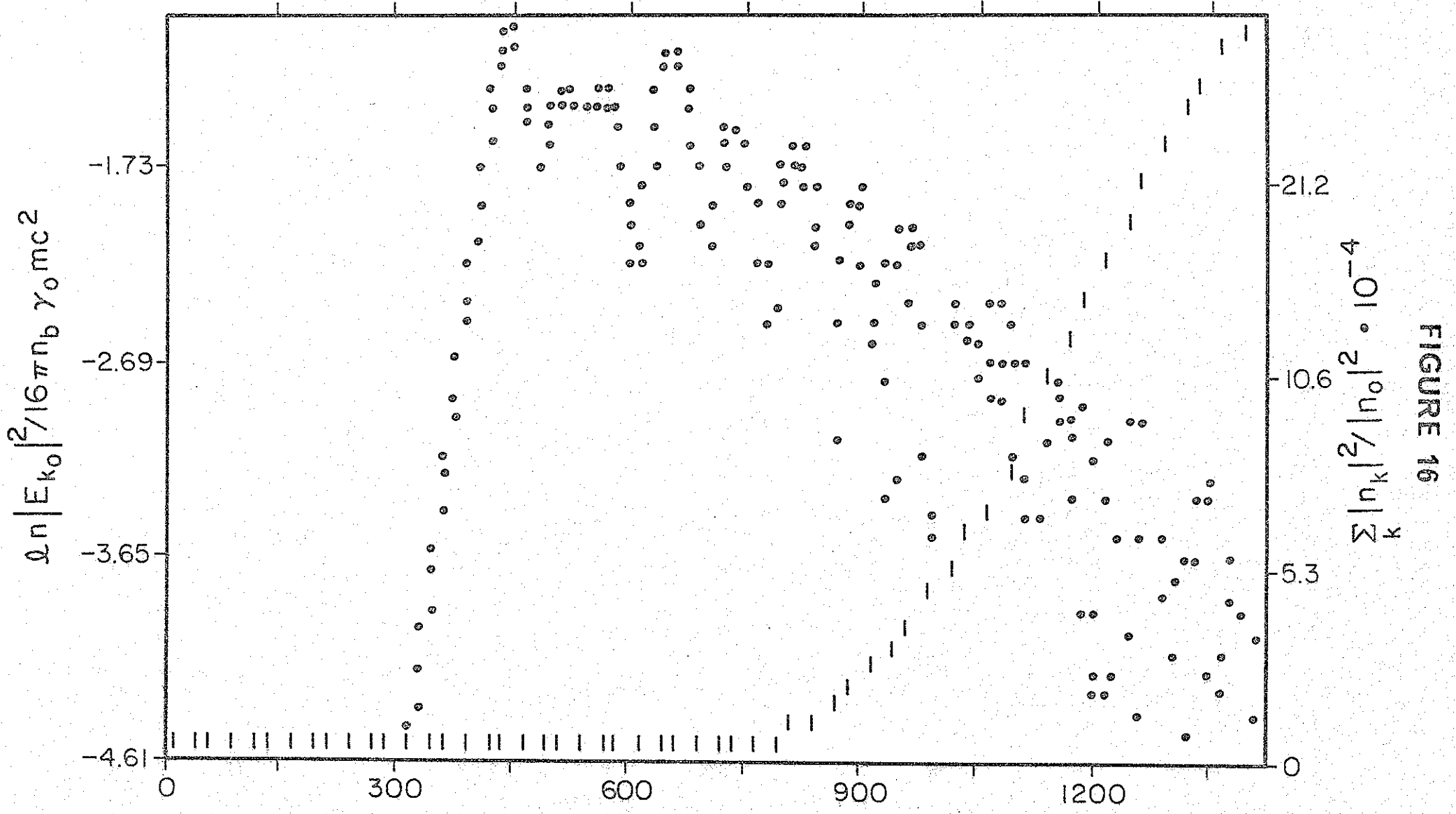
$\Omega n |E_{k_0}|^2 / 16\pi n_b \gamma_0 mc^2$
-1.73
-2.69
-3.65
-4.61
0
300
600
900
1200
21.2
10.6
5.3
0
$\Sigma_k |n_k|^2 / |n_0|^2 \cdot 10^{-4}$

FIGURE 16

FIGURE 17

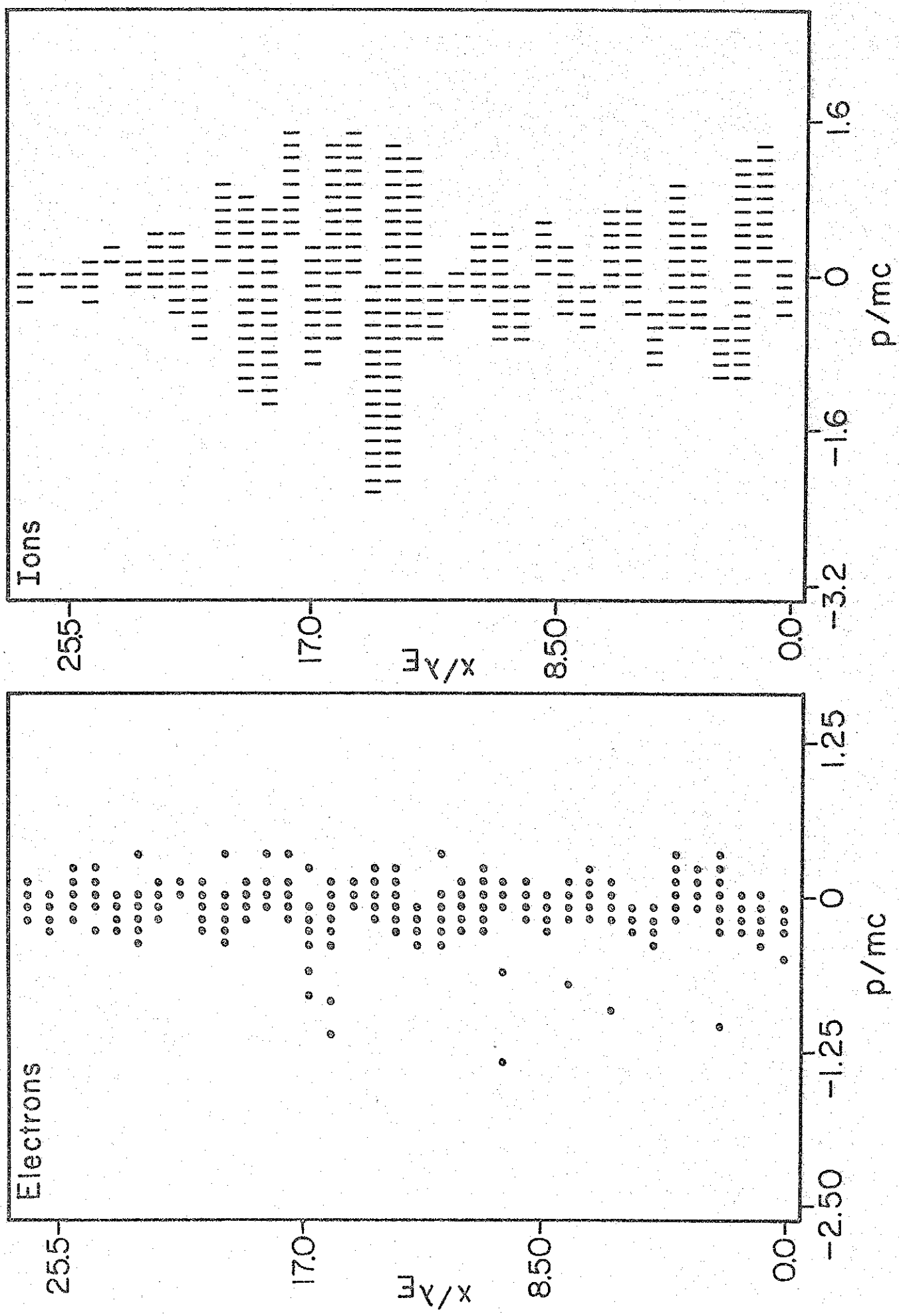
Ions
255.
170.
85.0
0.0
x/λE
1.6
0
-1.6
-3.2
p/mc
Electrons
255.
170.
85.0
0.0
x/λE
1.25
0
-1.25
-2.50
p/mc

FIGURE 18

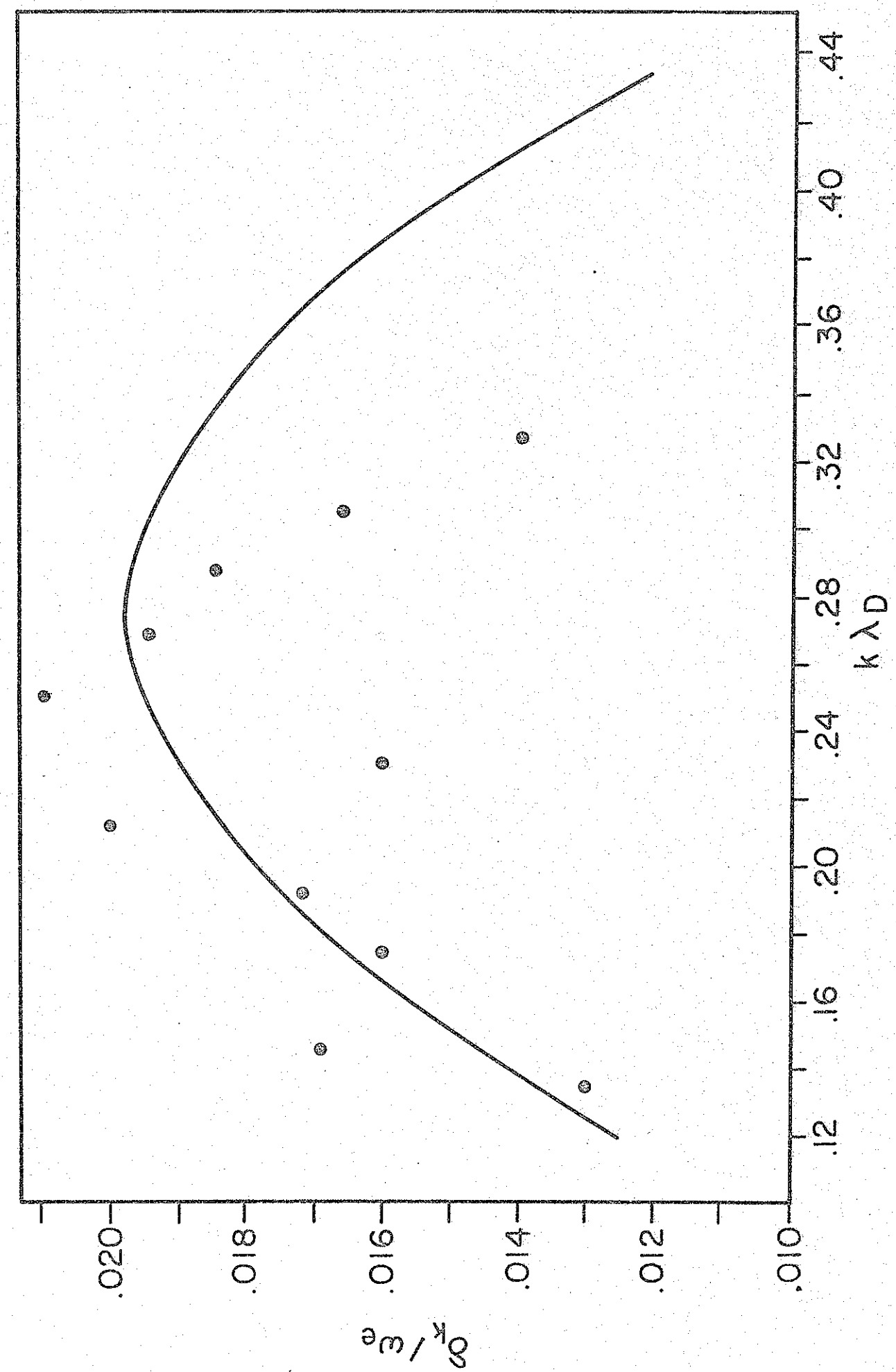
.020
.018
.016
.014
.012
.010
δ_k/ω_e
.12
.16
.20
.24
.28
.32
.36
.40
.44
$k\lambda_D$

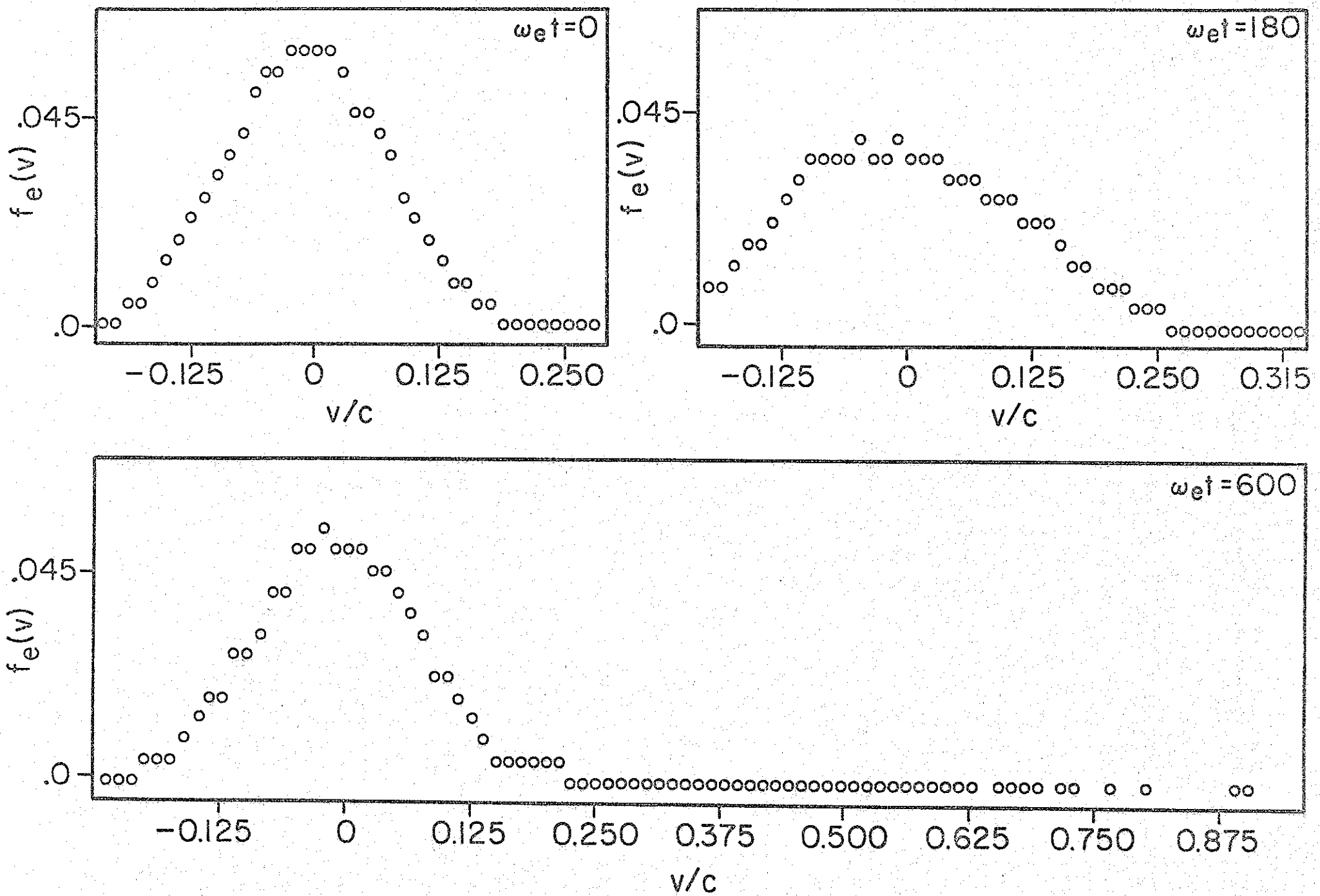
$\omega_e t = 0$
$\omega_e t = 180$
$\omega_e t = 600$
$f_e(v)$
.045
.0
−0.125
0
0.125
0.250
0.315
0.375
0.500
0.625
0.750
0.875
v/c

FIGURE 19

FIGURE 20

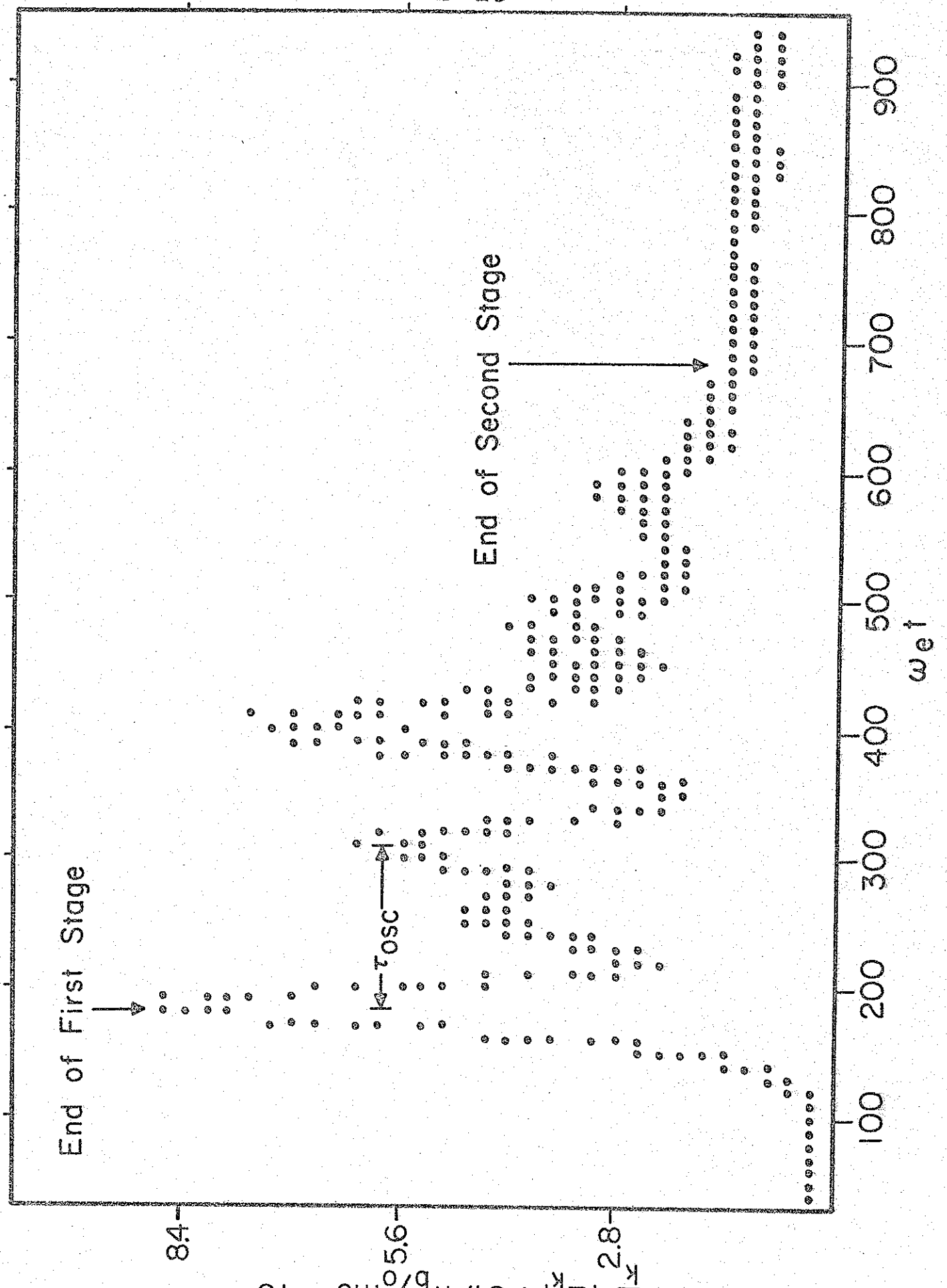
End of First Stage
End of Second Stage
τ_{osc}
$\omega_e t$
100
200
300
400
500
600
700
800
900
2.8
5.6
8.4
$\sum_k |E_k|^2/8\pi n_b \gamma_0 mc^2 \cdot 10^{-2}$

FIGURE 21

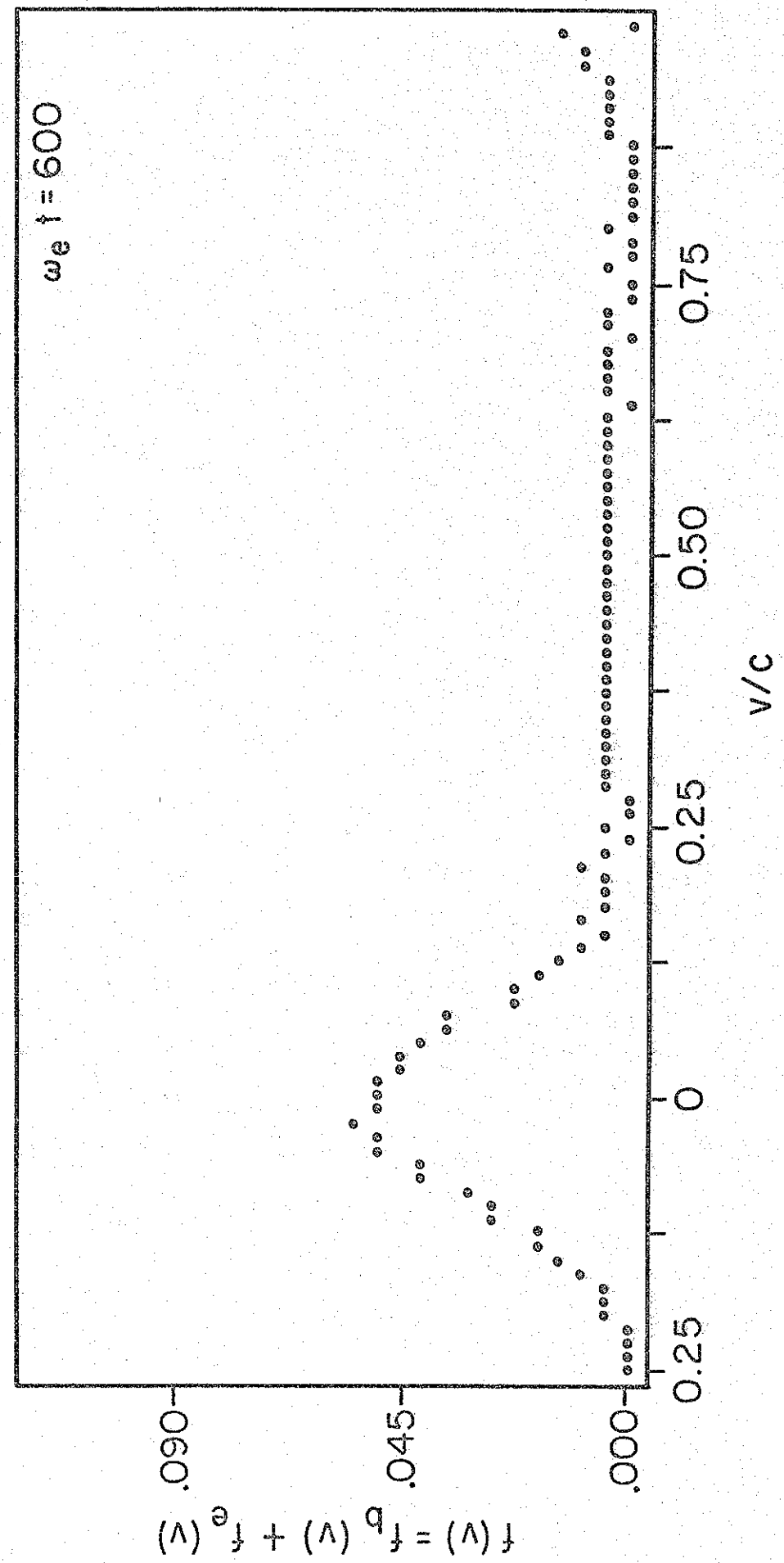

FIGURE 22

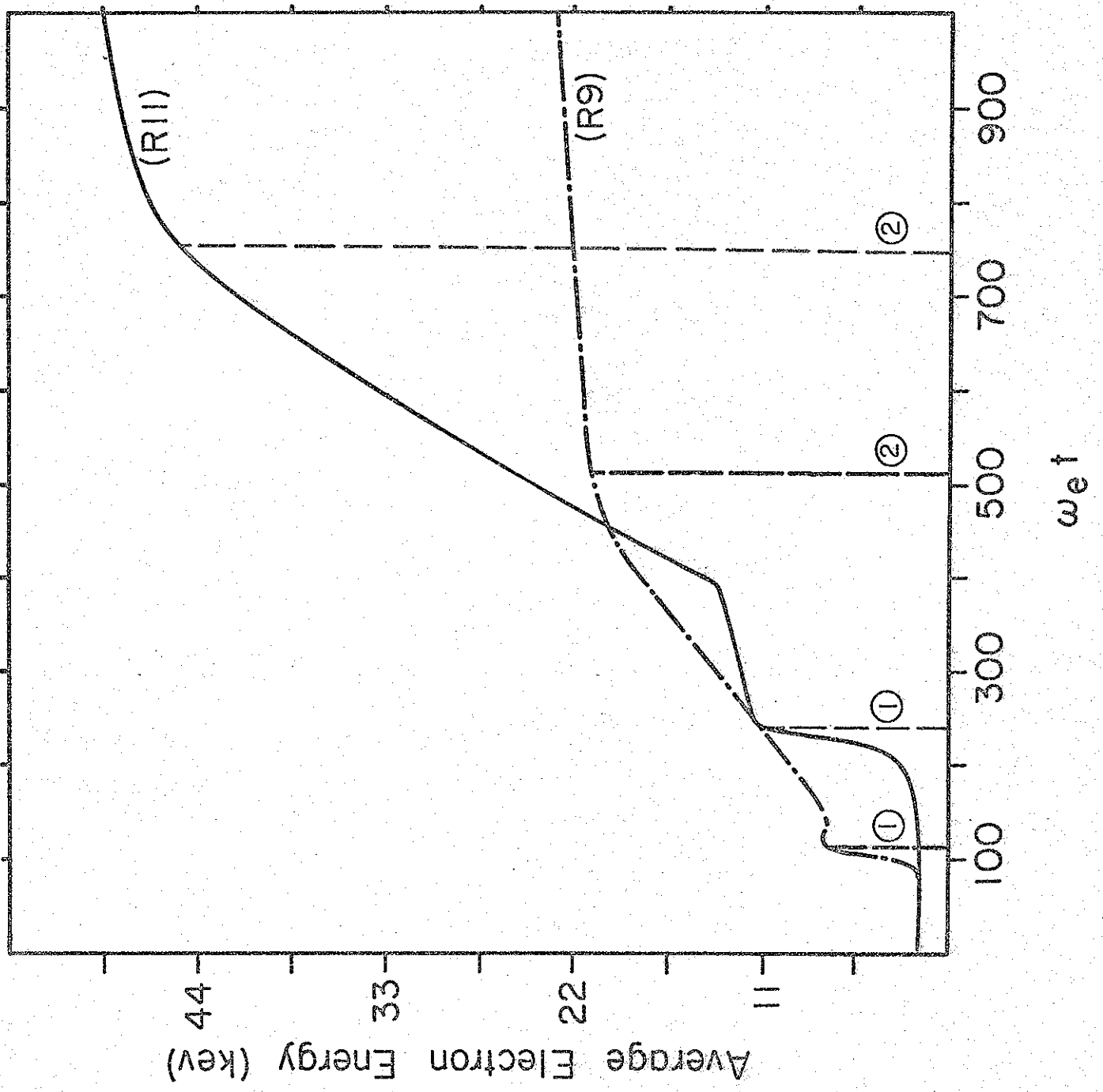
(R11)
(R9)
②
②
①
①
100
300
500
700
900
$\omega_e t$
11
22
33
44
Average Electron Energy (kev)

FIGURE 23

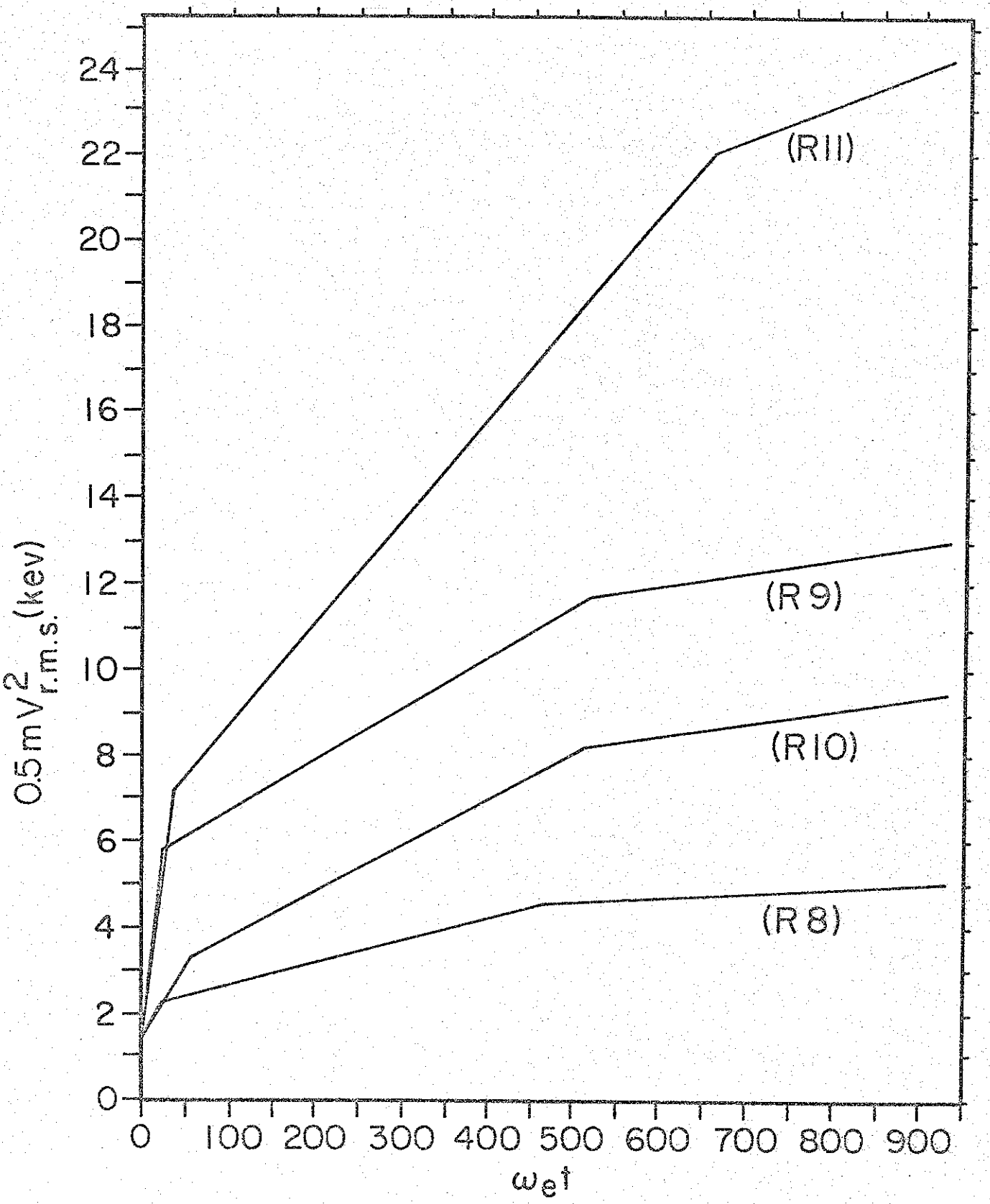
24
22
20
18
16
14
12
10
8
6
4
2
0
0 100 200 300 400 500 600 700 800 900
$\omega_e t$
$0.5 m V^2_{r.m.s.}$ (kev)
(R11)
(R 9)
(R10)
(R 8)